Investigating the cis-regulatory mechanisms underlying neuronal imprinted expression

HARVARD UNIVERSITY
Graduate School of Arts and Sciences

DISSERTATION ACCEPTANCE CERTIFICATE

The undersigned, appointed by the

Department of Molecular and Cellular Biology

have examined a dissertation entitled

Investigating the cis-regulatory mechanisms underlying neuronal imprinted expression

presented by Daniel Loftus

candidate for the degree of Doctor of Philosophy and hereby certify that it is worthy of acceptance.

Signature Victoria D'Souza (Dec 14, 2023 13:17 EST)

Typed name: Prof. Victoria D'Souza

Signature

Typed name: Prof. Catherine Dulac

Signature Brian Liau (Dec 15, 2023 11:05 EST)

Typed name: Prof. Brian Liau

Date: December 14, 2023

Investigating the cis-regulatory mechanisms underlying neuronal imprinted expression

A dissertation presented

by

Daniel Loftus

to

The Department of Molecular and Cellular Biology

In partial fulfillment of the requirements for the degree of

Doctor of Philosophy

in the subject of

Cell and Molecular Biology

Harvard University

Cambridge, Massachusetts

October 2023

Dissertation Advisor: Dr. Amanda Whipple Daniel Loftus

Investigating the cis-regulatory mechanisms underlying neuronal imprinted expression

ABSTRACT

Differences in chromatin state inherited from the parental gametes influence the regulation of maternal and paternal alleles in offspring. This phenomenon, known as genomic imprinting, results in genes preferentially transcribed from one parental allele. While local epigenetic factors such as DNA methylation are known to be important for the establishment of imprinted gene expression, less is known about the mechanisms by which differentially methylated regions (DMRs) lead to differences in allelic expression across broad stretches of chromatin. Allele-specific higher-order chromatin structure has been observed at multiple imprinted loci, consistent with the observation of allelic binding of the chromatin-organizing factor CTCF at multiple DMRs. However, whether allelic chromatin structure impacts allelic gene expression is not known for most imprinted loci. Here we characterize the mechanisms underlying brain-specific imprinted expression of the *Peg13-Kcnk9* locus, an imprinted region associated with intellectual disability. We performed region capture Hi-C on mouse brain from reciprocal hybrid crosses and found imprinted higher-order chromatin structure caused by the allelic binding of CTCF to the *Peg13* DMR. Using an *in vitro* neuron differentiation system, we showed that imprinted chromatin structure precedes imprinted expression at the locus. Additionally, activation of a distal enhancer induced imprinted expression of *Kcnk9* in an allelic chromatin structure-dependent manner. This work provides a high-resolution map of imprinted chromatin structure and demonstrates that chromatin state established in early development can promote imprinted expression upon differentiation.

ACKNOWLEDGEMENTS

I would first like to thank my advisor, Dr. Amanda J. Whipple, for her support throughout this process. It has been a huge honor to be the first graduate student of the Whipple Lab, and it is an experience I will forever cherish. I am grateful for her willingness to allow me to develop a new research focus for the lab based on my interest in higher-order chromatin structure, and for mentoring and guiding me along the way. In addition to sharing her deep knowledge of genomic imprinting, gene regulation, and molecular techniques with me, Dr. Whipple provided invaluable insights into how to form research questions, how to strategically and efficiently get to the heart of a scientific problem, and how to clearly communicate my results to a variety of different audiences. Overall, Dr. Whipple showed consistent personal investment in my development as a scientist and as a human being, and I would not be here today without her.

Additionally, I would like to thank the past and present members of the Whipple Lab that have provided support and companionship along the way. In particular, I would like to thank the following: Courtney Whilden, for her support with microscopy and for being a trusted friend throughout this process; Dr. Bongmin Bae, for joining the chromatin structure team, for the regular scientific discussions, and for always letting me use her reagents when I run out; Dr. Thareendra De Zoysa, for always jumping in to help without question and for his career advice; Udbhav Chitta, for his hard work, friendship, and ability to always lighten up the lab. An additional thank you to Dr. Michiko Inouye, Jen Yi, Aditya Wirawan, Carlie McGrath, Simon Schnabl, Daniel Blackwell, and Amanda Leinbaugh, all of whom enhanced my experience in the Whipple Lab in their own ways.

I would also like to thank the members of my committee, each of whom has been there starting with my qualifying exam, through all of my committee meetings, and finally at my defense. I would like to thank the chair of my committee, Dr. Victoria D'Souza, for always being

willing to meet with me and for providing critical advice at key moments during my PhD. I would also like to thank Dr. Catherine Dulac for her knowledge of genomic imprinting in the brain, for always pushing me, and for her consistently valuable insights during committee meetings. Finally, I would like to thank Dr. Brian Liau for his deep interest in my work and for providing such targeted feedback and conversations regarding chromatin structure, CTCF biology, and molecular methods.

I would also like to thank my family who have supported me and believed in me throughout the years. In particular I would like to thank my mom, LeAnn Loftus, for educating me from first grade through twelfth grade, and my dad, David Loftus for being such a strong intellectual role model in the way he approached problems and ideas. Additionally, I would like to thank my siblings for their roles in making me who I am today: to Rachel, for always being someone worth looking up to and providing such a high bar to reach for growing up; to Adrienne, for being one of my best friends, for sharing so much joy with me throughout the years, and for being so important to my choosing to become a scientist in the first place; to Jasper, for demonstrating so much courage and for showing me that a person's life is their own; to Andrew, for his passion and hard work and for always being willing to play a game of chess when I needed to unwind; and to Thomas, for your maturity and thoughtfulness that pushes me to be a better role model. I would also like to thank my Grandad, Wendell Dunlap, for his unwavering belief in the importance of education and for showing me the importance of hard work, focus, and service to others.

Finally, I would like to thank some of the friends that joined me along the way and played crucial roles in getting me to where I am today. To my best friend, Rudy Castellanos, I am eternally grateful for how he changed my life. No one outside of my parents has had the influence on me that Rudy has had. My friendship with him gave me the confidence and perspective to pursue this dream. He believed in me in ways that very few people did, and has

been one of my biggest sources of support through the many highs and lows. Additionally, I must thank Hassan Wang, a true kindred spirit if there ever was one. I would like to thank Hassan for the many hours of deep intellectual discussion and for always having something interesting to say. I have leaned upon Hassan during many critical moments during this journey, and I always walk away feeling better prepared to take the next steps. Last but not least, I would like to thank my partner Sianna Casey for her unwavering support during my PhD. She has helped me to perform at a level that I do not believe would have been possible without her.

TABLE OF CONTENTS

LIST OF FIGURES

LIST OF SUPPLEMENTAL TABLES

INTRODUCTION

Evolutionary and molecular basis of genomic imprinting

Prior to fertilization, the maternal and paternal genomes differ in multiple aspects of chromatin state, reflecting the unique processes of oogenesis and spermatogenesis (Guibert et al. 2012; Collombet et al. 2020; Smith et al. 2012). While most of these differences, which include DNA methylation, histone modifications, and higher-order chromatin structure, are equalized by epigenetic reprogramming in early embryogenesis, some withstand this process and are maintained throughout development (Xie et al. 2012; Monk 2015). These long-term imbalances in chromatin state between the parental alleles, known as genomic imprinting, result in parent-of-origin specific differences in transcriptional levels at approximately 200 genes in humans (Tucci et al. 2019; Ferguson-Smith and Bourc'his 2018) (Fig. 1). While genomic imprinting has provided an important model system for the study of an array of biological fields including epigenetics, noncoding RNA function, and sexual evolutionary dynamics, many basic questions regarding genomic imprinting remain poorly understood.

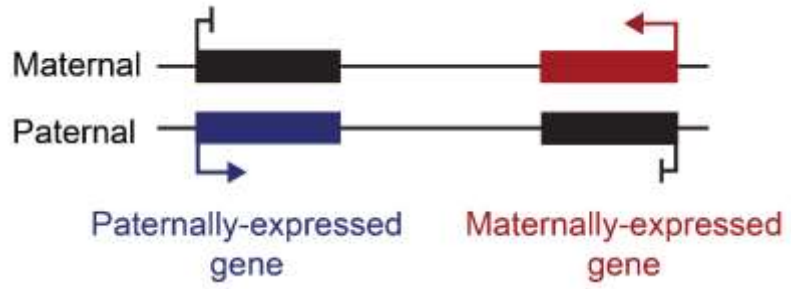

Figure 1 – Genomic imprinting
Cartoon showing imprinted gene expression. Red = maternal expression; blue = paternal expression; black = transcriptionally silent.

Genomic imprinting has been observed in diverse sexually-reproducing lineages including placental mammals, flowering plants (Raissig et al. 2011) and insects (Anaka et al. 2009). Although the evolutionary origins of genomic imprinting remain a matter of some debate,

one of the most successful models explaining the selective pressure behind the acquisition of imprinted expression of a particular gene is the genetic conflict theory (Haig 2000). This theory says that in a species with promiscuous sexual reproduction with high maternal resource investment in individual offspring, the optimal behavior of the offspring will be different for male and female parents. The female, which is equally related to all maternal offspring, has an evolutionary incentive for as many offspring as possible to survive and reproduce. The male, on the other hand, is not related to its offspring's half siblings, and therefore these half siblings are direct competitors of the male's offspring when it comes to acquiring maternal resources. Consequently, gene expression patterns that lead to a higher consumption of maternal resources are favorable to the paternal genome, while expression patterns that lead to a more equitable distribution of maternal resources to all offspring are favorable to the maternal genome. As a result of this competition between males and females as well as between rival males, there is evolutionary pressure for parent-of-origin specific expression of certain genes.

Mechanistically, genomic imprinting in mammals derives from differences in chromatin state between the maternally and paternally derived chromosomes. The male and female germ lines undergo extensive epigenetic reprogramming during gametogenesis (Messerschmidt et al. 2014). This provides each sex with the opportunity to optimize the epigenetic state of the germ cells for the benefit of the male or female reproductive strategy. However, because maternally-deposited factors within the oocyte are largely responsible for the epigenetic reprogramming that occurs during early embryogenesis, the maternal genome has the opportunity to drive this reprogramming. One particularly dramatic example of this is observed in several insect lineages, where whole paternally-derived chromosomes are eliminated during development, including during gametogenesis (Goday and Esteban 2001; Herbette and Ross 2023). In mammals, this early developmental power imbalance is observed in the differences in the rate of epigenetic reprogramming on the maternal and paternal genomes, with the paternal genome

experiencing active, rapid demethylation and the maternal genome experiencing passive, slower demethylation (Mayer et al. 2000; Gu et al. 2011). Consistent with this, most genomic regions with differences in DNA methylation between the parental genomes that survive epigenetic reprogramming have a methylated maternal allele and an unmethylated paternal allele (Li et al. 2018). Overall, it is this early embryonic reprogramming stage that provides the ultimate basis for genomic imprinting, with the epigenetic differences that survive this process having the opportunity to be inherited during cell division throughout differentiation and go on to drive allele-specific transcription patterns.

Tissue specificity of genomic imprinting in placental mammals

While imprinted expression is found across many developmental timepoints and tissues in placental mammals, it is especially prevalent during early embryogenesis. Imprinting is particularly well studied in the placenta and other early developmental extraembryonic tissue (Hanna 2020). This tissue is at the maternal-embryonic interface and plays an important role in regulating the transfer of resources from female to offspring, making it a natural front line in the genomic imprinting battle of the sexes according to genetic conflict theory. Among the first imprinted genes discovered in mammals were insulin-like growth factor 2 (*Igf2*) and its receptor *Igf2r* (Barlow et al. 1991; Ferguson-Smith et al. 1991). *Igf2* is an important embryonic growth factor that leads to an increase in embryonic growth, while *Igf2r* is a receptor that leads to the degradation of *Igf2* (Ghosh et al. 2003). Consistent with the genetic conflict theory, the growth-promoting *Igf2* is expressed exclusively from the paternal allele, while the growth-restricting *Igf2r* is expressed exclusively from the maternal allele. Extraembryonic tissue also has the most diverse chromatin mechanisms of genomic imprinting thus far identified in placental mammals. While all embryonic genomic imprinting known to date is mediated by allelic differences in DNA methylation, the repressive histone modification H3K27me3 has been shown to play a role in

the paternal-specific expression of several genes in extraembryonic tissue (Inoue et al. 2017), further highlighting the importance of imprinted expression in these lineages.

In addition to extraembryonic tissue, mammalian genomic imprinting is especially prevalent in the developing and adult brain (Perez et al. 2015), and many neurodevelopmental disorders are associated with the dysregulation of imprinted genes (Perez et al. 2016; Isles 2022). Because many imprinted genes are exclusively expressed from one parental allele, heterozygous deletions or mutations in this allele can lead to a complete loss of expression of the imprinted gene, often with severe consequences. For example, at the well-studied 15q11-q13 imprinted locus, maternal deletions lead to the neurodevelopmental disorder Angelman syndrome, while paternal deletions lead to a distinct disorder known as Prader-Willi syndrome (Cassidy et al. 2000). Angelman syndrome is caused by the loss of expression of the maternally expressed ubiquitin ligase *Ube3a*. This gene is normally active on the maternal allele and silenced on the paternal allele due to transcriptional interference of the paternal-specific antisense transcript *Ube3a-AS*. Recent work to activate paternal *Ube3a* through the use of antisense oligonucleotides (ASOs) to knock down *Ube3a-ATS* has shown promise (Meng et al. 2015; Dindot et al. 2023), highlighting the importance of understanding the molecular mechanisms underlying imprinted expression to treat imprinting disorders. The precise molecular cause of Prader-Willi syndrome is less clear, although genetic mapping of the causal paternally-derived deletions has isolated a small region encompassing the SNORD116 small nucleolar RNA (snoRNA) cluster as the minimal sufficient deletion (Bieth et al. 2015). These genetically similar but phenotypically distinct diseases highlight the importance of understanding the genetics and molecular mechanisms underlying imprinted disorders in order to treat human disease.

DNA methylation as the epigenetic basis of genomic imprinting

An early observation regarding genomic imprinting was that imprinted genes are not randomly distributed across the genome, but rather tend to occur in clusters (Cattanach and Kirk 1985). These large genomic clusters, often exceeding a megabase in size, are linked to the presence of differentially methylated regions (DMRs) known as imprint control regions (ICRs) that are typically a few kilobases or less (Gigante et al. 2019). DNA methylation is an epigenetic mark in which the 5-position of a cytosine nucleotide is methylated (Fig. 2A). DNA methylation is

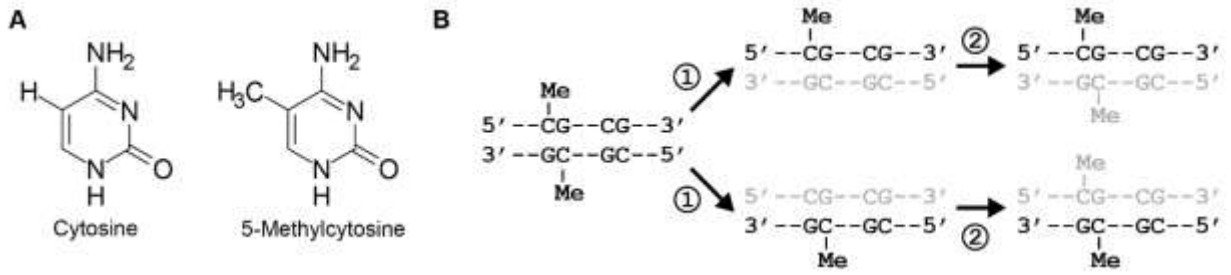

Figure 2 – DNA methylation
A. Chemical structure of cytosine (left) and 5-methylcytosine (right). **B.** Inheritance of DNA methylation state following DNA replication. Step 1: Following DNA replication, each of the daughter double helices will inherit one strand from the original helix (black), which preserves the methylation state of the parent, and one newly synthesized strand (grey), which is unmethylated. Step 2: DNMT1 recognizes hemimethylated CpGs and methylates the unmethylated cytosine, thus restoring the methylation state of the parental double helix.

most often found in the palindromic CpG dinucleotide context, although low levels of cytosine methylation are observed in other sequence contexts (Xie et al. 2012). *De novo* DNA methylation on unmethylated cytosines is primarily catalyzed by the methyltransferases DNMT3A and DNMT3B (Moore et al. 2013). These methyltransferases catalyze the methylation of both cytosines at a CpG site, one on each of the two strands of the DNA double helix. Following DNA replication, the two new copies of double-stranded DNA will each have one methylated cytosine on the template strand and one unmethylated cytosine on the newly synthesized strand (Fig. 2B). This hemimethylated state is recognized by a separate maintenance methyltransferase, DNMT1, which catalyzes the methylation of the unmethylated

cytosine (Moore et al. 2013). Through this method, the original methylation state is inherited by both daughter DNA strands, making DNA methylation a robustly heritable epigenetic mark. DNA methylation can be removed either passively by inhibiting the action of DNMT1, thus leading to a dilution in methylation over successive DNA replications, or actively by the oxidation of methylated cytosine by TET proteins.

In mammals, most cytosines in a CpG context are methylated, with approximately 60-80% of CpG cytosines being methylated depending on the tissue type (Xie et al. 2012). The major exception to this trend is at CpG islands (CGIs), which are typically found at gene promoters, have a high density of CpG, and tend to have low levels of methylation. Outside of CGIs, there is a general depletion of CpG dinucleotides genome wide (Beck et al.). This is likely due to the increased mutagenic tendency of methylated cytosines. Cytosines are subject to spontaneous or enzymatic deamination (Krokan et al. 2002). While the deamination of unmethylated cytosines creates uracils that can be recognized by the DNA repair machinery and corrected, deamination of methylated cytosine creates thymines which are not as efficiently recognized as mutations by the repair machinery (Lindahl 1993).

Mechanisms of DNA methylation-mediated chromatin silencing

DNA methylation is an important repressive epigenetic mark in most eukaryotes and is involved a wide array of genome silencing functions including the induction and maintenance of constitutive heterochromatin, repressing transposable elements, and the silencing of some gene promoters (Mattei et al. 2022). DNA methylation leads to chromatin repression by a variety of mechanisms (Héberlé and Bardet 2019). Methylated cytosine can directly block activating transcription factors from binding to DNA, preventing them from recruiting the transcriptional machinery. On the other hand, many repressive proteins have a high affinity specifically for methylated DNA. For example, the highly conserved methyl-CpG-binding domain (MBD) domain is found on many DNA binding proteins such as MeCP2, which can be used to recruit

repressive chromatin modifiers to DNA (Fuks et al. 2003b). DNA methylation can also cooperate with other repressive epigenetic marks and associated factors to further induce chromatin silencing. DNA methylation frequently colocalizes with the repressive histone mark H3K9me3, an important feature of constitutive heterochromatin, and the two repressive marks can mutually reinforce each other. For example, DNMT3A binds to the H3K9me3 methyltransferase SUV39H1 as well as well characterized heterochromatin proteins such as HP1 (Fuks et al. 2003a). DNMT1 can also be recruited to chromatin by H3K9me3, thus reinforcing the maintenance of heterochromatin during cell division (Ren et al. 2020). Conversely, active histone marks such as H3K4me3 may play a role in preventing DNA methylation at active promoters and enhancers. DNMT3A has a high affinity for unmethylated H3K4, but much lower affinity for H3K4me3 (Otani et al. 2009). Interestingly, deletion of the H3K4 demethylase LSD1 leads to a global loss of DNA methylation due to reduced DNMT1 stability, further highlighting the relationship between these systems (Wang et al. 2009). Finally, DNA methylation is also antagonistic with facultative polycomb-induced heterochromatin. Polycomb domains, which are often found at unmethylated CpG islands and marked with the repressive histone marks H3K27me3 and H2AK119ub1, are associated with the facultative silencing of lineage specific developmental genes. Loss of DNA methylation leads to a gain of H3K27me3 throughout the genome, suggesting that DNA methylation prevents H3K27me3 (Hagarman et al. 2013). Additionally, loss of the DNA demethylase Tet1 leads to a loss of the H3K27 methyltransferase Ezh2 at gene promoters along with a concomitant reduction in H3K27me3 (Chrysanthou et al. 2022). Overall, DNA methylation is a central repressive epigenetic mark in mammalian cells, which along with its high heritability during cell division makes it an ideal epigenetic mark for the maintenance of genomic imprinting.

Developmental dynamics of DNA methylation

DNA methylation is highly dynamic throughout development (Fig. 3). There are two major epigenetic reprogramming phases that take place during the mammalian life cycle, one during gametogenesis and one following fertilization (Messerschmidt et al. 2014). Primordial germ cells (PGCs) undergo a wave of demethylation, resetting the epigenetic state for the next generation (Seisenberger et al. 2012). Following demethylation, there is a remethylation phase

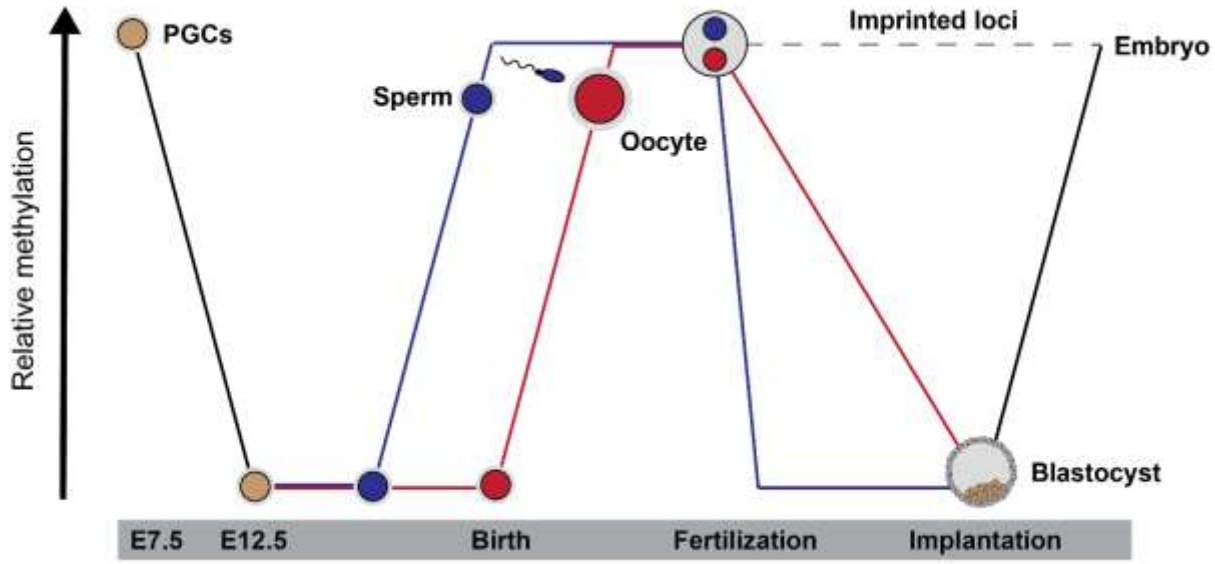

Figure 3 – Developmental dynamics of DNA methylation
Schematic showing global DNA methylation dynamics during mammalian development. Two waves of global DNA methylation occur, one during gametogenesis and one following fertilization. Imprinted loci are resistant to the post-fertilization wave of demethylation, allowing for parent-of-origin specific DNA methylation profiles.

that leads to different methylation patterns in males and females (Kota and Feil 2010). While the differences in methylation established during this remethylation phase provide the ultimate basis for the parental differences in DNA methylation that will become the basis of imprinted gene expression in the embryo, many more DMRs are detected between sperm and oocyte than are detected in the offspring following embryogenesis (Smallwood et al. 2011). The final set of DMRs that go on to become ICRs is determined during the second wave of epigenetic

reprogramming that occurs following fertilization. During this process there is another global wave of demethylation that occurs through different rates and mechanisms on the maternal and paternal DNA, with paternal DNA being demethylated more rapidly that maternal DNA (Mayer et al. 2000; Gu et al. 2011). ICRs are resistant to this global wave of DNA methylation erasure that occurs in the early embryo (Messerschmidt et al. 2012; Li et al. 2008). The KRAB zinc finger protein ZFP57 has been identified as an essential factor for protecting allelic DNA methylation at ICRs, and humans with mutations in *Zfp57* display hypomethylation at multiple ICRs (Li et al. 2008; Mackay et al. 2008). Additional factors such as TRIM28 have been shown to be important for ICR maintenance both before and after epigenetic reprogramming as well (Messerschmidt et al. 2012; Alexander et al. 2015, 28).

Higher-order chromatin structure and enhancer-mediated transcription regulation

In addition to factors such as DNA methylation and histone modification that play a crucial role in the accessibility of chromatin on nucleosomal scale, the higher-order structure of genomic regions on the kilobase to megabase scale can also play an important role in transcription regulation (Rao et al. 2014). The interactions between cis-regulatory elements such as promoters, enhancers, and insulators within a given genomic neighborhood often determine whether the nearby genes are silenced or expressed. Enhancers are regulatory sequences whose function is to regulate the expression of nearby genes. There are far more enhancers than genes within mammalian genomes, and developmentally regulated genes are typically regulated by multiple enhancers (Donnard et al. 2018; González et al. 2015). Enhancers share many of the characteristics of promoters (Spicuglia and Vanhille 2012). They are bound by transcription factors, contain low levels of DNA methylation, display active histone marks such as H3K27 acetylation and H3K4 methylation, and are transcribed by RNA polymerase II. The RNAs that are generated by enhancers tend to be short-lived and

bidirectionally transcribed, and enhancer transcription correlates with transcription at genes regulated by the enhancers (Mahat et al. 2023). Many disease-causing SNPs are located within enhancers, emphasizing the important role they play in gene expression (Claringbould and Zaugg 2021).

The mechanisms by which enhancers activate nearby genes remains a subject of significant research. Enhancers are capable of regulated genes hundreds of kilobases away, and yet which genes a particular enhancer regulates can be tightly regulated, with some enhancers regulating certain nearby genes and not others (Vangala et al. 2020). In recent years, it has become clear that higher-order chromatin folding patterns can play a significant role in determining enhancer-promoter communication patterns. The use of techniques such as Hi-C has revealed that chromatin folds into hierarchical regions of high-contact frequency known as topologically associating domains (TADs) (Rao et al. 2014) (Fig. 4A,B). Enhancers tend to be

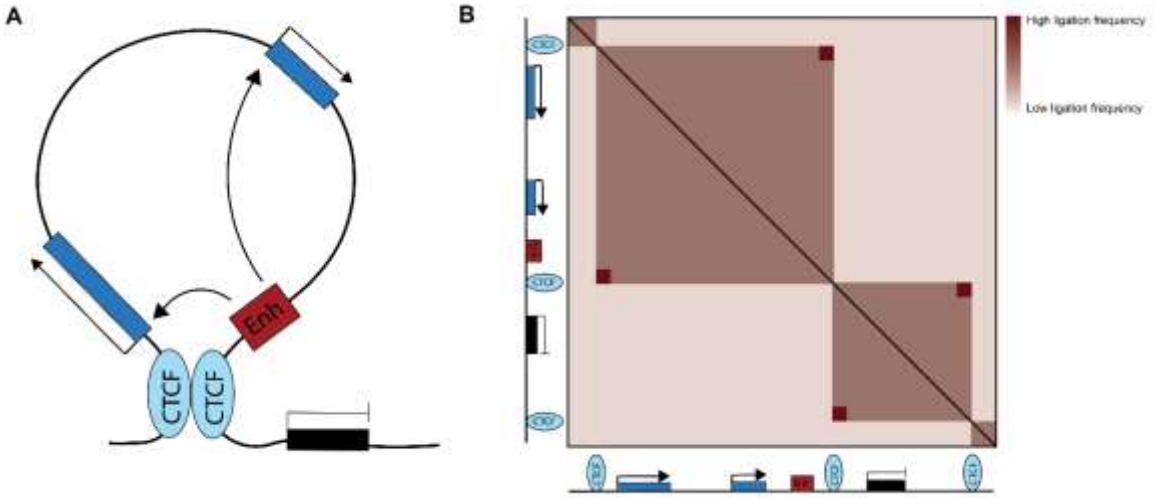

Figure 4 – TADs as revealed by Hi-C
A. Cartoon of a topologically associating domain (TAD) showing restricted enhancer activity. **B.** Theoretical Hi-C results showing the TAD from A.

found within the same TAD as the promoters that they regulate, and genes within individual TADs have correlated levels of gene expression (Dily et al. 2014). High resolution Hi-C and other techniques derived from it show that in addition to TADs there are individual contacts between distal genomic regions that can be mapped to nucleosome depleted regions on the chromatin (Krietenstein et al. 2020). While TADs are mostly formed early in development and are relatively stable during differentiation, individual contacts can be more dynamic and correlate with the activation of tissue-specific gene expression (Bonev et al. 2017).

The role of CTCF in regulating higher-order chromatin structure

Among the most important determinants of chromatin structure in mammalian cells is the DNA-binding protein CTCF. CTCF is usually found at TAD boundaries and is known for its ability to insulate promoters from surrounding enhancers (Rao et al. 2014; Bell et al. 1999). CTCF is thought to mediate higher-order chromatin structure by acting as barrier to the loop extrusion processivity of the cohesin complex, causing CTCF and cohesin subunits to colocalize at TAD boundaries (Davidson et al. 2019). Acute depletion of CTCF or cohesin leads to a sharp decrease in TAD structure genome-wide (Nora et al. 2017; Hyle et al. 2019). Interestingly, while techniques such as Hi-C that take the average chromatin structure of large numbers of cells are highly reproducible with regards to overall TAD structures, single-cell methods including Hi-C based techniques as well as microscopy reveal that CTCF-mediated loops are highly dynamic, and only a fraction of individual chromosomes at a time show the loops observed in bulk Hi-C (Tan et al. 2018; Wang et al. 2016). Thus Hi-C maps are more a measure of contact frequency between genomic regions than they are a picture of a static structure. Theoretical work on models of transcription regulation show that the distance-expression relationship between enhancers and promoters can be explained by a model whereby transient contacts between promoters and enhancers can lead to robust transcriptional outputs, providing insight into the mechanisms by which enhancers affect promoters (Zuin et al. 2022). However, the precise role

of higher-order chromatin structure remains a matter of debate. While many individual examples of the importance of CTCF-mediated chromatin structure on gene expression exist (Ushiki et al. 2021; Gombert and Krumm 2009; Lupiáñez et al. 2015), severe ablation of native chromatin structure through the acute depletion of CTCF produces only modest changes in global gene expression (Nora et al. 2017; Hyle et al. 2019), leading to questions about the precise role of CTCF and higher-order chromatin structure more broadly in regulating transcription.

Higher-order chromatin structure and genomic imprinting

Studies of genomic imprinting have played an important part in our understanding of CTCF-mediated chromatin folding. Most notably, the *H19-Igf2* locus has long served as a critical model system for CTCF function, higher-order chromatin structure, and enhancer-mediated gene regulation (DeChiara et al. 1991; Bartolomei et al. 1991; Szabó et al. 2000). Early studies of the *H19-Igf2* locus found that CTCF binds only the unmethylated maternal ICR and plays multiple roles in regulating imprinted expression at the locus (Singh et al. 2012). First, allelic binding of CTCF leads to allelic higher-order chromatin structure at the *H19-Igf2* locus, thereby regulating imprinted gene expression through parent-of-origin differences in enhancer-promoter contacts (Kurukuti et al. 2006; Llères et al. 2019). Second, allelic CTCF binding to the maternal allele is essential for maintaining the unmethylated state of the ICR and surrounding secondary DMRs (Pant et al. 2004). Third, CTCF is important for maintaining allelic differences in histone modifications at the locus (Han et al. 2008). Allelic CTCF binding has since been shown to occur at many imprinted loci, which often correlates with allele-specific chromatin folding patterns. For example, allelic higher-order chromatin structure has been implicated in regulating imprinted expression at the murine *Dlk1-Dio3* and *Grb10-Ddc* loci (Llères et al. 2019; Juan et al. 2022). Additionally, recent work has revealed that allelic chromatin structure is present at multiple imprinted loci in human (Richer et al. 2023). However, whether this allelic chromatin

folding is functionally important for allelic gene expression has not been determined at most imprinted clusters.

Long noncoding RNAs in genomic imprinting

Imprinted clusters are enriched for noncoding RNAs, including lncRNAs, snoRNA, and miRNAs. Genomic imprinting has served as an important model system for the understanding of these noncoding RNA classes, with some of the best studied lncRNAs originating from imprinted gene clusters (Di Michele et al. 2023). Imprinted lncRNAs are especially well known for their role in mediating gene repression *in cis*, both through the recruitment of repressive chromatin complexes to surrounding genomic loci and through transcriptional interference (Pandey et al. 2008; Nagano et al. 2008; Meng et al. 2013; Sanli et al. 2018). The paternal-specific lncRNAs *Kcnq1ot1* and *Airn* mediate polycomb repression of the surrounding genes on the paternal allele in at their respective loci in extraembryonic tissue in a manner that is also dependent on pre-existing chromatin structure (Pandey et al. 2008; Nagano et al. 2008; Schertzer et al. 2019). Interestingly, the mechanisms of silencing by these lncRNAs has similarities to that of *Xist*, the well-characterized lncRNA that is important for mediating X-chromosome inactivation (XCI) (Statello et al. 2021). XCI itself is achieved in an imprinted manner in extraembryonic tissue (Engel 2015). Upon fertilization, the paternal X chromosome is condensed and silenced while the maternal X chromosome is open. In the extraembryonic lineages, this imprinted XCI is maintained while in the embryonic lineages the paternal X chromosome undergoes decondensation, after which random XCI is initiated.

In addition to chromatin level repression, cis-acting lncRNAs can also act through transcriptional interference, where the transcription of the lncRNA through a protein-coding gene can disrupt the transcription of the protein-coding gene (Di Michele et al. 2023). One example, mentioned above, is *Ube3a-ATS*, which is exclusively transcribed from the paternal and disrupts the transcription of *Ube3a* on the paternal allele, leading to maternal bias in *Ube3a* expression.

Another example of transcriptional interference is the antisense transcript *Nespas*, which overlaps the *Nesp* gene and is transcribed exclusively from the paternal allele (Williamson et al. 2006). This leads to maternal-specific expression of *Nesp* in a manner that is dependent upon *Nespas* transcription across the *Nesp* promoter (Tibbit et al. 2015). Finally, the paternal *Airn* acts to repress the expression of *Igf2r* by transcribing over the *Igf2r* promoter, causing silencing of *Igf2r* on the paternal allele (Latos et al. 2012). *Airn* provides an example of an imprinted cis-repressive lncRNA that works by both modes, with its silencing of *Igf2r* coming from transcriptional interference and its repression of more distal genes in the locus like *Slc22a2* and *Slc22a3* coming from the recruitment of repressive complexes to the chromatin. These examples demonstrate that lncRNAs or their transcription can act *in cis* to repress the transcription of surrounding genes through a variety of mechanisms, and can serve as a potent means of transmitting the epigenetic information contained the ICRs to surrounding chromatin.

The *Peg13-Kcnk9* imprinted cluster

One poorly understood imprinted cluster that potentially combines many of the themes discussed above, including brain-specific imprinting, DNA methylation, higher-order chromatin structure, and cis-repressive lncRNAs is the *Peg13-Kcnk9* imprinted locus (Fig. 5). The *Peg13-*

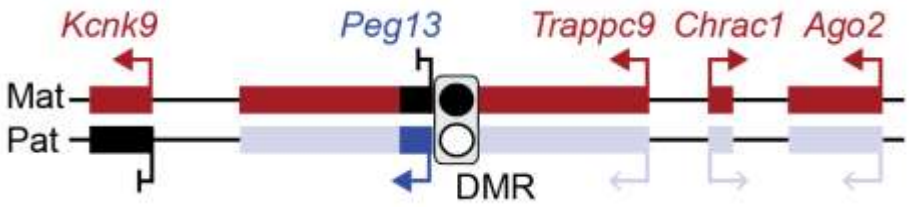

Figure 5 – The *Peg13-Kcnk9* imprinted cluster
The *Peg13-Kcnk9* imprinted cluster is composed of the paternally expressed lncRNA *Peg13*, the maternally expressed protein-coding gene *Kcnk9*, and the maternally biased protein-coding genes *Trappc9*, *Chrac1*, and *Ago2*. The locus DMR overlaps the *Peg13* promoter region (filled circle = methylated DMR; open circle = unmethylated DMR).

Kcnk9 imprinted locus is composed of the protein-coding genes *Kcnk9*, *Trappc9*, *Chrac1*, and *Ago2*, as well as the lncRNA *Peg13*. Imprinted expression of the locus has been observed in murine brain tissue but not in body tissues (Perez et al. 2015; Smith et al. 2003; Ruf et al. 2007; Court et al. 2014). More specifically, in mouse brain tissue, *Kcnk9* is expressed exclusively from the maternal allele, *Peg13* is expressed exclusively from the paternal allele, and *Trappc9*, *Chrac1*, and *Ago2* exhibit a maternal bias. In body tissues, *Kcnk9* and *Peg13* are transcriptionally silent, and *Trappc9*, *Chrac1*, and *Ago2* are expressed in a biallelic manner. *Peg13* is located within an intron of the large *Trappc9* gene, and is transcribed in an intronless manner in the sense direction relative to *Trappc9*. A maternally methylated DMR overlaps the promoter of *Peg13* (Smith et al. 2003; Xie et al. 2012) and is the putative ICR controlling imprinted expression of the entire locus (Court et al. 2014; Singh et al. 2011). Although the protein coding genes found at the *Peg13-Kcnk9* locus are conserved across mammals, with the basic genomic structure found in mammals ranging from humans to mice to cows, the acquisition of the DMR and the *Peg13* lncRNA into the intron of *Trappc9* appears to be a more recent phenomenon that occurred in the ancestor of the Euarchontoglires (Suzuki et al. 2011; Chen et al. 2016). *Peg13* expression and imprinting of the surrounding protein coding genes is therefore restricted to this clade, which includes mouse and human.

Birk-Barel syndrome

Genetic mutations within the *Peg13-Kcnk9* cluster are associated with intellectual disability (Marangi et al. 2013; Abbasi et al. 2017; Mortreux et al. 2018), most notably Birk-Barel syndrome, which is caused by maternal inheritance of a missense mutation in the potassium leak channel *Kcnk9* (Barel et al. 2008). Birk-Barel syndrome is a rare genetic disorder caused by missense mutations in the potassium leak channel *Kcnk9*. This disease can by caused by a variety of *Kcnk9* mutations; while G236R and R131H are the most common causal mutations to be identified, at least 17 unique mutations associated with Birk-Barel disease have been

identified within the coding region of *Kcnk9* (Cousin et al. 2022). *Kcnk9* is only expressed from the maternally inherited allele, and therefore Birk-Barel syndrome only occurs when the missense mutation is inherited maternally. While the majority of cases that have been identified are due to maternal inheritance of the causal mutation, cases where the mutation arose de novo in the affected individual rather than being inherited from the mother have also been identified (Cousin et al. 2022).

Patients with Birk-Barel syndrome display significant intellectual disability, hypotonia, and facial dysmorphia (Barel et al. 2008). As a potassium leak channel, *Kcnk9* plays an important role in setting the resting membrane potential of neurons. Electrophysiological studies of *Kcnk9* in xenopus oocytes show that unlike WT *Kcnk9*, mutant *Kcnk9* with the pathological G236R mutation does not produce a measurable current in voltage clamp studies. The G236R mutation is predicted to place a positively charged arginine residue within the ion conductance channel of the protein. Co-expression of WT *Kcnk9* with the G236R mutant leads to a decrease in conductance relative to WT alone, suggesting that the G236R mutation may act in a dominant-negative fashion (Barel et al. 2008). However, co-expression of WT and mutant do lead to higher overall conductance compared to no expression controls, suggesting that activation of WT paternal *Kcnk9* in Birk-Barel patients may be a strategy to provide some relief of the associated symptoms. However, knockout studies in mice reveal that loss of *Knck9* leads to impaired neuronal migration during cortical development (Bando et al. 2014), and so intervention early in development in patients with mutant *Kcnk9* may be critical. Despite this, a detailed understanding of the mechanisms underlying imprinted expression of *Kcnk9* and the *Peg13-Kcnk9* imprinted locus is still lacking.

Potential mechanisms underlying imprinted expression of the *Peg13-Kcnk9* locus

While the *Peg13* DMR is the putative ICR, the mechanisms by which it mediates the imprinted expression of surrounding genes is not known. Two major models are possible based on what is known from previously characterized imprinted loci. The first is a model by which allelic higher-order chromatin structure leads to allelic enhancer-promoter contacts, thus resulting in allelic expression. Allele-specific binding of CTCF has been observed at the *Peg13* DMR (Prickett et al. 2013), and previous studies have shown that the human CTCF binding site has insulator activity (Court et al. 2014). The second model is one in which the *Peg13* lncRNA mediates silencing of the surrounding genes on the paternal allele in a cis-repressive manner. This model is consistent with the observation that imprinted of the maternally-biased protein-coding genes is only observed in brain, which coincides with the brain-specific expression of *Peg13*. These two models are not mutually exclusive, and it is possible that different genes in the locus are regulated by different mechanisms, as is the case with the *Airn-Igf2r* locus.

Here we characterize the role of allelic CTCF binding and chromatin structure at the murine *Peg13-Kcnk9* imprinted locus. We performed region capture Hi-C on brain tissue from reciprocal hybrid mouse crosses and found differences in TAD boundaries, insulation, and enhancer-promoter contact frequency between the two parental alleles due to allelic CTCF binding at the *Peg13* DMR. Deletion of the paternal CTCF binding sites at the *Peg13* DMR in an *in vitro* neuron differentiation system led to a maternalization of paternal chromatin structure, loss of the *Peg13* lncRNA, and an accompanying loss of *Peg13-Kcnk9* locus imprinted expression. Moreover, we found that imprinted chromatin structure precedes imprinted expression at the locus, and that pre-existing allelic chromatin structure is sufficient to induce maternal-specific expression of *Kcnk9* upon activation of distal enhancers. This work contributes to our understanding of how higher-order chromatin structure can regulate tissue-specific imprinted expression and has broad implications for the role of pre-existing chromatin structure in developmental gene expression.

RESULTS

Chromatin structure at the *Peg13-Kcnk9* locus is imprinted

The *Peg13-Kcnk9* locus is composed of the lncRNA gene *Peg13* and the protein-coding genes *Kcnk9*, *Trappc9*, *Chrac1*, and *Ago2* (Fig. 6A). Imprinted expression of the locus has been observed in murine brain tissue but not in body tissues (Perez et al. 2015; Smith et al. 2003; Ruf et al. 2007; Court et al. 2014). More specifically, in mouse brain tissue, *Kcnk9* is expressed exclusively from the maternal allele, *Peg13* is expressed exclusively from the paternal allele, and *Trappc9*, *Chrac1*, and *Ago2* exhibit a maternal bias. In body tissues, *Kcnk9* and *Peg13* are transcriptionally silent, and *Trappc9*, *Chrac1*, and *Ago2* are expressed in a biallelic manner. A

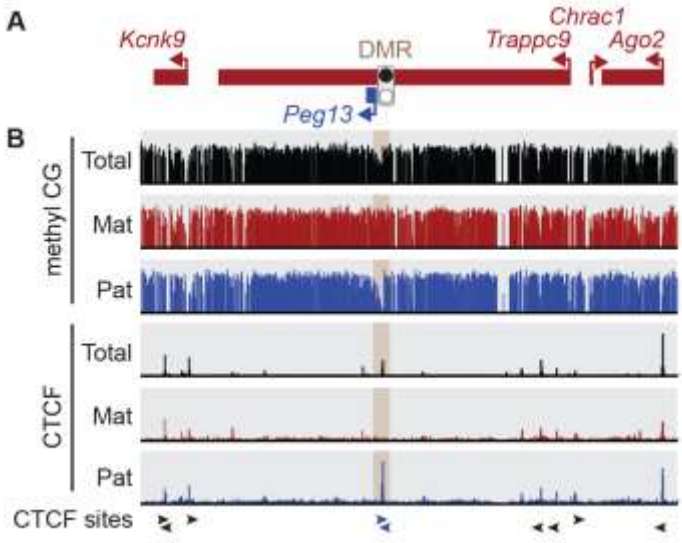

Figure 6 – The *Peg13-Kcnk9* imprinted locus
A. The structure of the murine *Peg13-Kcnk9* locus. **B.** Allelic CpG methylation (reanalyzed from Xie et al., 2012) and allelic CTCF binding (reanalyzed from Prickett et al., 2013) at the *Peg13-Kcnk9* locus in mouse brain.

maternally methylated DMR overlaps the promoter of *Peg13* (Fig. 6B) (Xie et al. 2012) and is the putative ICR controlling imprinted expression of the entire locus (Court et al. 2014; Singh et

al. 2011). While paternal-specific expression of *Peg13* is almost certainly due to the DMR at its promoter, it is not known how imprinted expression of the distal genes is achieved, or why imprinted expression is exclusively observed in the brain. Analysis of publicly available CTCF ChIP-seq datasets from mouse brain showed paternal-specific CTCF binding at the *Peg13* DMR (Fig. 6B) (Prickett et al. 2013), consistent with the known antagonistic relationship between DNA methylation and CTCF binding (Wang et al. 2012; Damaschke et al. 2020; Luo et al. 2021) and previous observations in human brain tissue (Court et al. 2014).

In order to determine if allelic CTCF binding at the *Peg13* DMR results in allelic chromatin structure, we generated reciprocal mouse crosses of the distantly related mouse strains *M.m.musculus* (B6) and *M.m.castaneus* (CAST). Leveraging single-nucleotide polymorphisms (SNPs) to distinguish between the B6 and CAST genomes, we first developed an allele-specific droplet-digital PCR (ddPCR) assay (Fig. 7A-D) and observed the expected imprinted expression of *Kcnk9*, *Peg13*, *Trappc9*, and *Ago2* in reciprocal mouse brain tissue (Fig. 7E). *Chrac1* does not contain any exonic SNPs and was therefore excluded from analysis. We then performed region capture Hi-C on brain tissue from reciprocal hybrid crosses using biotinylated capture probes to 1.5 Mb of chromatin at the *Peg13-Kcnk9* imprinted locus and neighboring genes. Seventy-two percent of Hi-C read pairs contained strain-specific SNPs and were used to generate allelic contact maps. The allelic contact maps were highly reproducible between biological replicates (Fig. 8A) and merged for further analysis. Allelic contact maps showed clear differences in the chromatin contacts between the maternal and paternal genomes across the *Peg13-Kcnk9* locus in both crosses (Fig. 8B). To isolate parent-of-origin effects from strain effects, allelic reads from the reciprocal crosses were randomly downsampled to the same depth and merged by parent-of-origin (Fig. 8C). On the maternal allele a single TAD crossing the DMR predominates, anchored by a strong contact between the *Kcnk9* transcription start site (TSS) and a distal region in an intron of *Trappc9* (Fig. 8C,

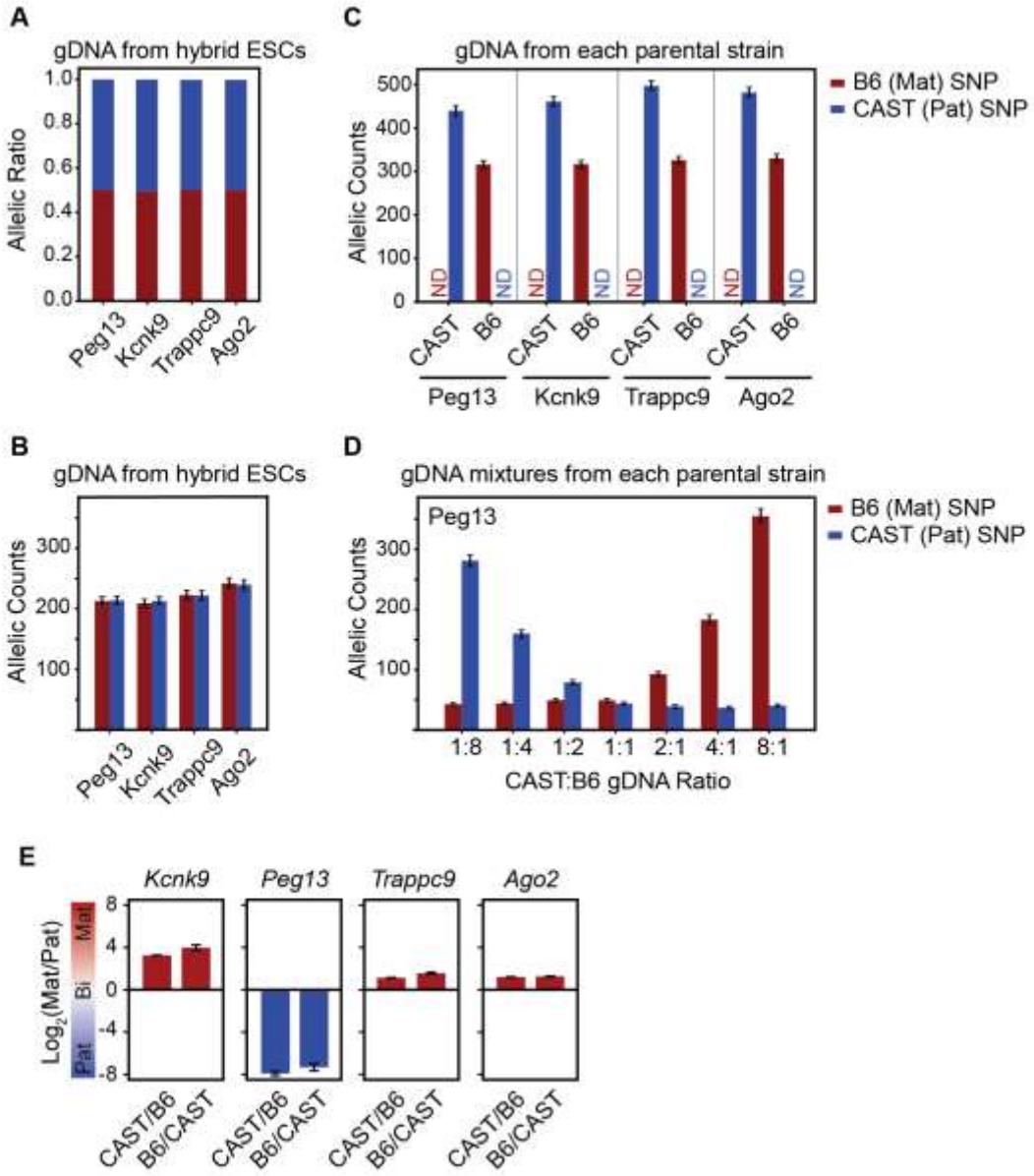

Figure 7 – Allele-specific droplet-digital PCR accurately demonstrates imprinted expression at the *Peg13-Kcnk9* locus

A-B. Allelic ddPCR for each of the indicated genes on genomic DNA from hybrid mouse embryonic stem cells (ESCs) showing maternal to paternal allelic ratio (A) and allelic counts (B). **C.** Allelic ddPCR for each of the indicated genes on genomic DNA from B6 or CAST strains. ND, not detected. **D.** Allelic ddPCR for *Peg13* on genomic DNA from B6 or CAST strains mixed at the indicated ratios. Error bars, Poisson 95% confidence interval. **E.** Ratio of maternal to paternal expression in brain tissue from reciprocal hybrid mouse crosses as measured by RT-ddPCR. Note that biallelic expression is when y = 0. Mean ± SEM (n=3).

arrowhead ‘a’). On the paternal allele, this TAD is less pronounced and two additional smaller, paternal-specific TADs are observed that are anchored at the CTCF-bound *Peg13* DMR (Fig. 8C, arrowheads ‘b’ and ‘c’). Long-range, paternal-specific contacts anchored at the DMR are also seen (Fig. 8C, arrowheads ‘d’ and ‘e’), as well as a weak paternal-specific contact between the DMR and the *Ago2* TSS (Fig. 8C, arrowhead ‘f’).

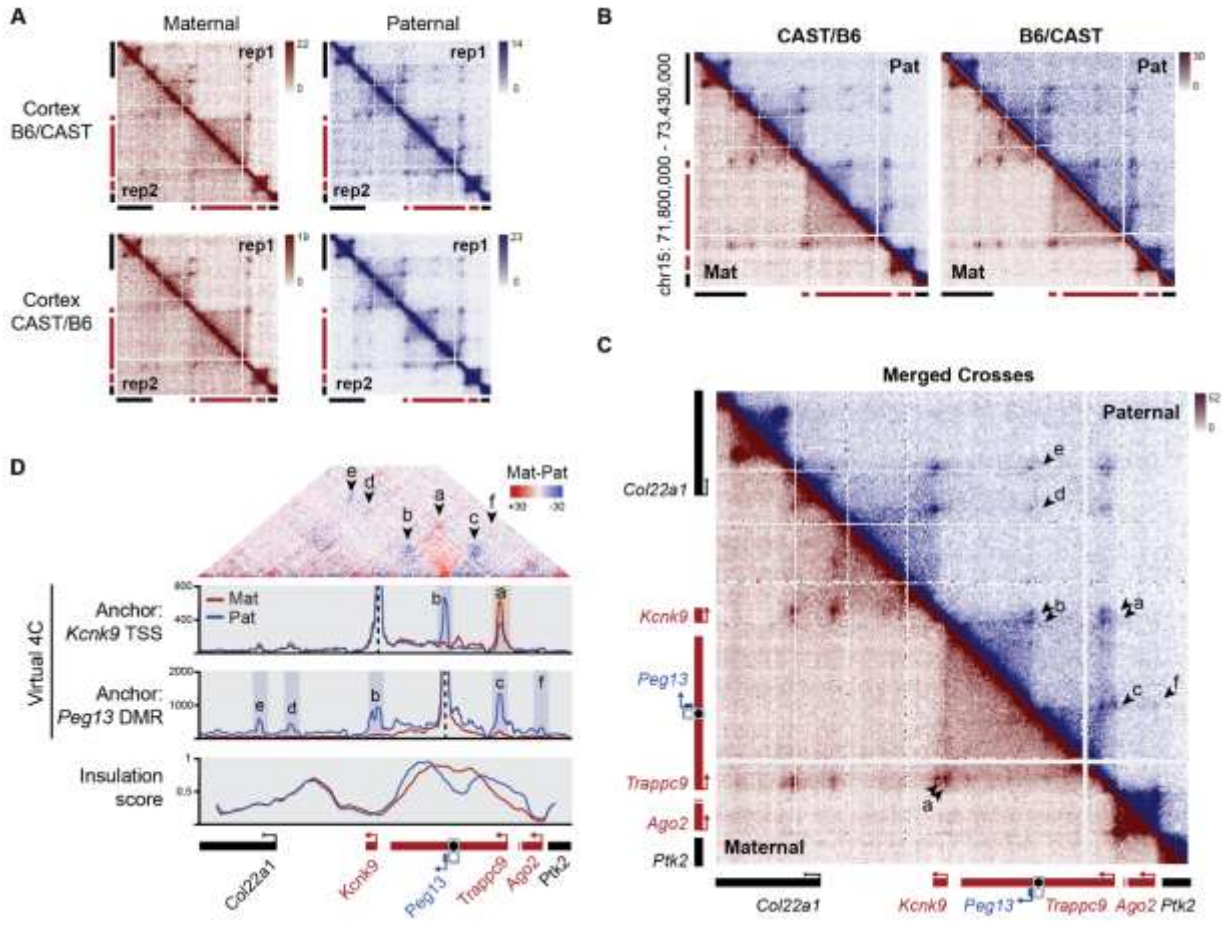

Figure 8 – Chromatin structure at the *Peg13-Kcnk9* locus is imprinted
A. Comparison of region capture Hi-C maps between biological replicates for each hybrid cross and parental allele. **B.** Allelic contact maps from region capture Hi-C of reciprocal hybrid mouse brain. **C.** Merged allelic contact maps combining both crosses from (C). Arrowheads indicate contacts of interest. **D.** (Top) Hi-C subtraction plots (maternal – paternal) showing allelic biased contacts. (Middle) Virtual 4C analysis of the region capture Hi-C datasets anchored at the *Kcnk9* TSS or the *Peg13* DMR. Contacts of interest are highlighted. (Bottom) Allelic insulation score analysis.

The parental bias in contacts across the imprinted locus can be further visualized as allelic subtraction maps (maternal minus paternal reads) (Fig. 8D, top). This view reveals that contacts crossing the *Peg13* DMR are less frequent on the paternal allele. This reflects the insulating effect of paternal-specific CTCF binding and is consistent with previous results showing that the human *Peg13* DMR has insulator activity (Court et al. 2014). We additionally performed virtual 4C analysis of the allelic Hi-C data from two anchor points, the *Kcnk9* TSS and the DMR (Fig. 8D, middle). Using the *Kcnk9* TSS as the anchor, we confirmed a maternally biased contact with the *Trappc9* intronic region (arrowhead 'a') and a paternal-specific contact with the DMR (arrowhead 'b'). Using the DMR as the anchor, we confirmed that all major contacts made by the DMR are paternal-specific (arrowheads 'c'-'f'), thereby demonstrating the strong effect of paternal-specific CTCF binding at the unmethylated DMR. Finally, allelic insulation score analysis highlights the paternal-specific TAD boundary at the *Peg13* DMR (Fig. 8D, bottom). These results provide a high-resolution view of imprinted chromatin structure at the *Peg13-Kcnk9* locus and are consistent with allelic CTCF binding at the *Peg13* DMR as the basis of the structural differences between the two parental alleles.

Imprinted chromatin structure precedes imprinted expression at the *Peg13-Kcnk9* locus

To investigate the mechanisms regulating brain-specific imprinted expression at the *Peg13-Kcnk9* locus, we implemented an *in vitro* neuron differentiation system from hybrid mouse embryonic stem cells (ESCs) which is amenable to allelic measurements and rapid genetic perturbations (Whipple et al. 2020). Briefly, ESCs were derived from a B6 x CAST cross. Hybrid ESCs were then differentiated into induced neurons (iNs) by doxycycline-inducible expression of *Ngn2* for 6-12 days. Successful differentiation was noted by appearance of

neuronal cell morphology (Fig. 9A) in addition to down-regulation of the pluripotency genes *Nanog* and *Oct3/4* and upregulation of the neuronal marker *Tubb3* (Fig. 9B).

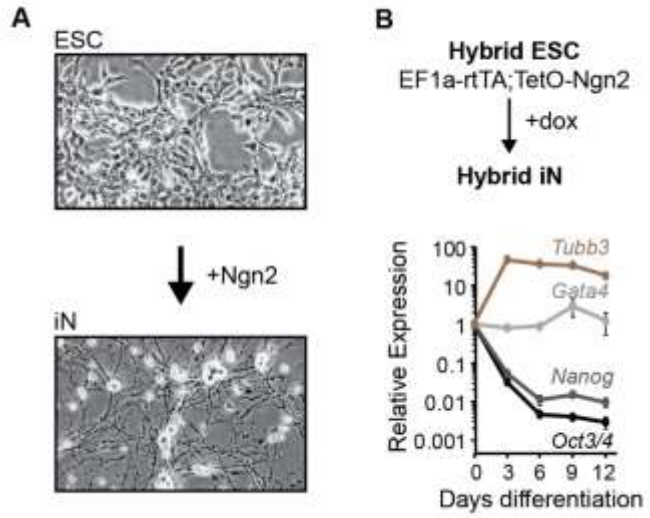

Figure 9 – Allele-specific *in vitro* neuron differentiation
A. Light microscopy showing ESCs and iNs. **B.** RT-qPCR of pluripotency and differentiation marker genes during *in vitro* neuron differentiation.

We first characterized allelic DNA methylation and gene expression patterns at the *Peg13-Kcnk9* locus during neuron differentiation. Targeted nanopore sequencing of native genomic DNA in ESCs and iNs at the *Peg13* DMR showed >90% methylation on the maternal allele and 25-50% methylation on the paternal allele (Fig. 10A,B), a finding which was corroborated using bisulfite Sanger sequencing (Fig. 10C). RT-qPCR showed that *Kcnk9* and *Peg13* are robustly upregulated during neuron differentiation, with modest upregulation of *Trappc9* and *Ago2* (Fig. 10D). ddPCR showed that the expression of *Kcnk9* is strongly maternal in iNs and *Peg13* is strongly paternal (Fig. 10E). *Trappc9* and *Ago2* are bi-allelically expressed in ESCs and acquire a maternal bias upon neuron differentiation (Fig. 10E). The parental bias in expression of all four genes in iNs is similar to mouse brain tissue. These results show that imprinted expression of the *Peg13-Kcnk9* locus is acquired during neuron differentiation in the

absence of changes in methylation at the DMR (Fig. 10F). This, therefore, provides a good model system to interrogate the mechanistic basis of cell type-specific imprinted expression.

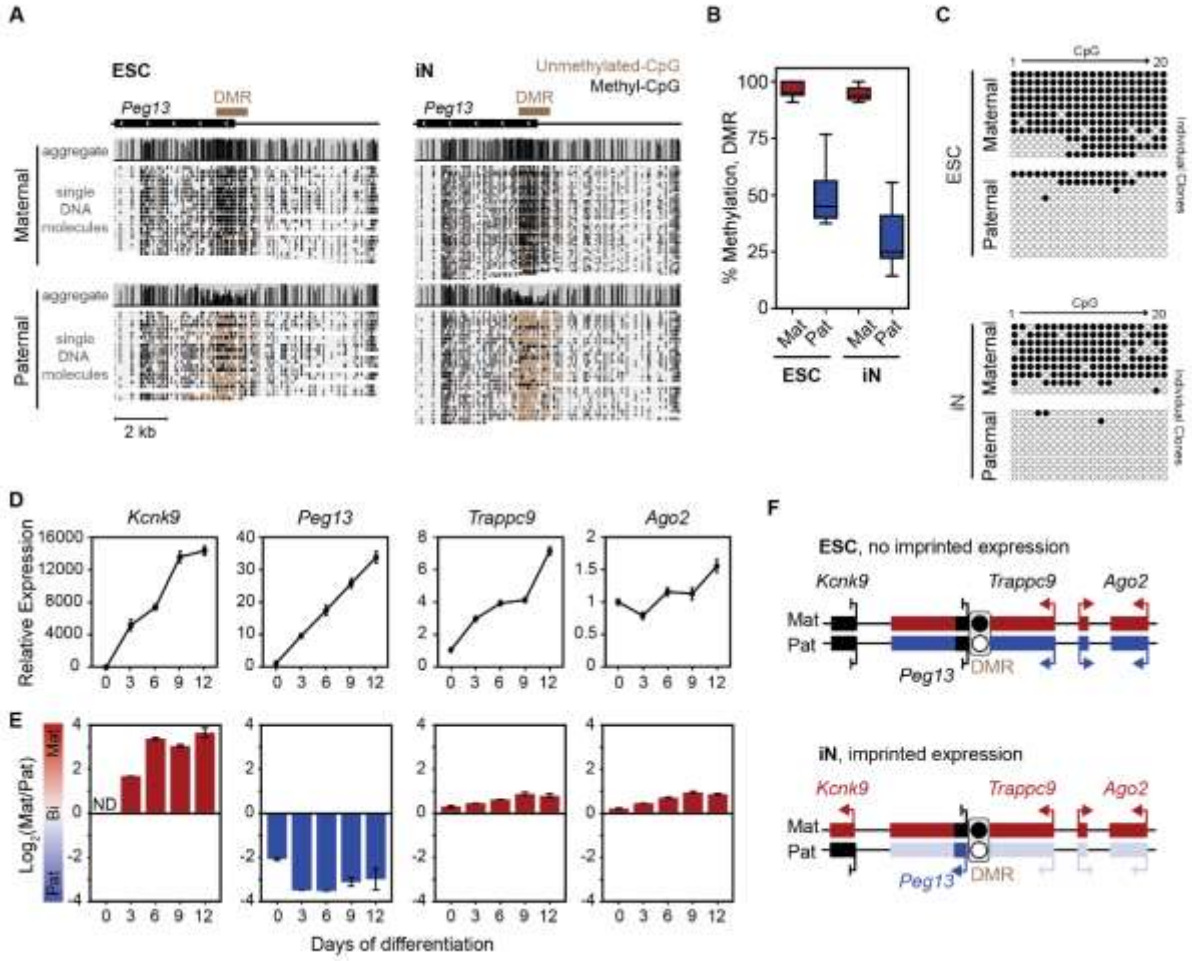

Figure 10 – Imprinted expression of the *Peg13-Kcnk9* locus is acquired during neuron differentiation

A. Targeted nanopore sequencing of native genomic DNA to measure allelic DNA methylation levels at the *Peg13* DMR in ESCs and iNs. **B.** Quantification of average methylation levels at individual CpGs at the DMR from (A). **C.** Bisulfite Sanger-sequencing in ESCs and iNs indicating methylated (closed circles) and unmethylated (open circles) CpGs. **D.** Relative total expression levels of the genes in the *Peg13-Kcnk9* locus during differentiation as measured by RT-qPCR. Mean ± SEM (n=3). **E.** RT-ddPCR during neuron differentiation. Mean ± SEM (n=3). ND, not detected. **F.** Diagram summarizing allelic DMR methylation and gene expression patterns in ESCs and iNs.

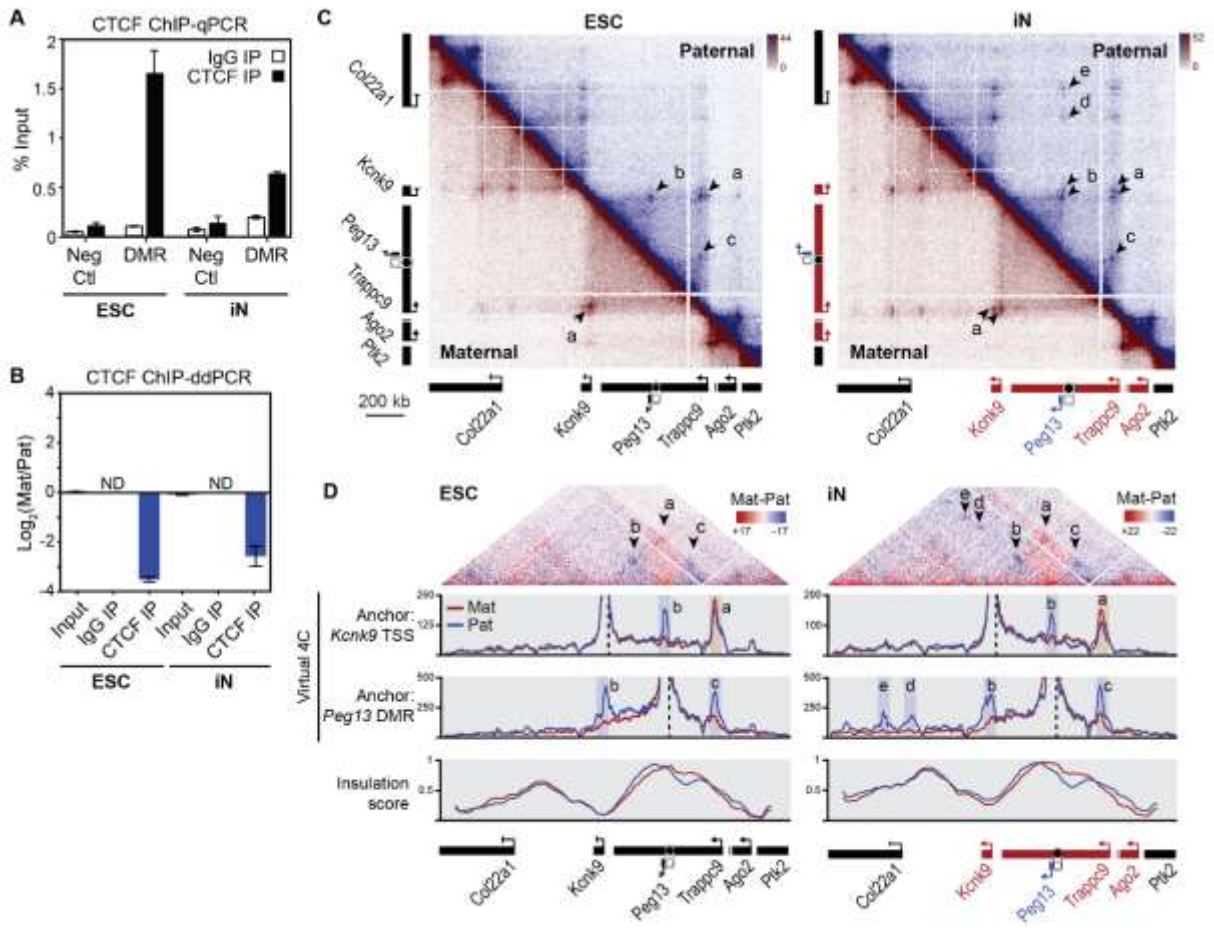

Figure 11 – Imprinted chromatin structure precedes imprinted expression at the *Peg13-Kcnk9* imprinted locus
A. CTCF ChIP-qPCR at the *Peg13* DMR and a non-CTCF bound control region (Neg Ctl) in ESCs and iNs. Mean ± SEM (n=3). **B.** ChIP-ddPCR for the allelic ratio of CTCF binding in ESCs and iNs. Mean ± SEM (n=3). ND, not detected. **C.** Allelic contact maps from region capture Hi-C in ESCs (left) and iNs (right). Arrowheads indicate contacts of interest. **D.** (Top) Hi-C subtraction plots (maternal – paternal) showing allelic biased contacts. (Middle) Virtual 4C analysis of the region capture Hi-C datasets anchored at the *Kcnk9* TSS or the *Peg13* DMR. Contacts of interest are highlighted. (Bottom) Allelic insulation score analysis.

We next examined how chromatin structure may change during neuron differentiation. First, we performed CTCF ChIP and found that CTCF binds to the *Peg13* DMR in a paternal-specific manner in both ESCs and iNs (Fig. 11A,B). We then performed region capture Hi-C before and after neuron differentiation. Like our *in vivo* studies, allelic contact maps were highly

reproducible between biological replicates (Fig. 12A). We observed imprinted chromatin structure in both ESCs and iNs, and major allelic contacts observed *in vivo* were also seen *in vitro* (Fig. 11C,D). The contact maps are largely similar between ESCs and iNs, with iNs exhibiting some strengthening of existing contacts at nearby CTCF sites (double arrowheads 'a' and 'b') and gain of additional long-range contacts between the paternal DMR and regions outside the imprinted domain (arrowheads 'd' and 'e'). This is further appreciated on subtraction maps (ESC – iN) for each allele (Fig. 12B). These results show that imprinted chromatin structure is already established in ESCs and precedes imprinted gene expression at the *Peg13-Kcnk9* locus.

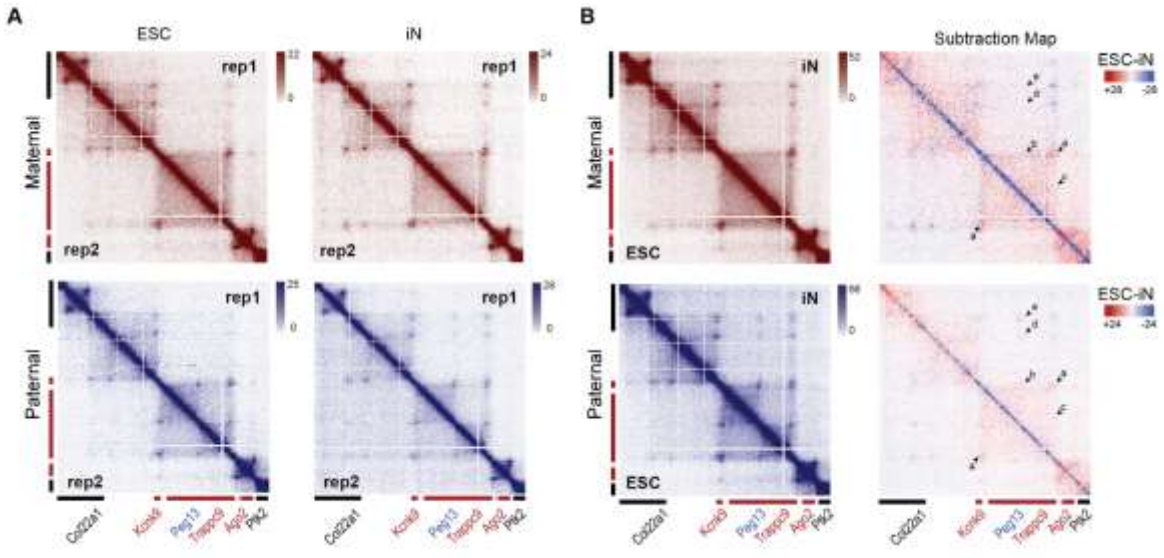

Figure 12 – Further analysis of ESC and iN region capture-Hi-C
A. Comparison of region capture Hi-C maps between biological replicates for ESCs and iNs. **B.** Hi-C subtraction plots (ESC – iN) showing cell type-biased contacts.

The CTCF region of the *Peg13* DMR is essential for imprinted expression

The *Peg13* DMR consists of approximately 2 kb of genomic sequence overlapping the *Peg13* promoter (Gigante et al. 2019). Given that this is the only DMR that has been identified in

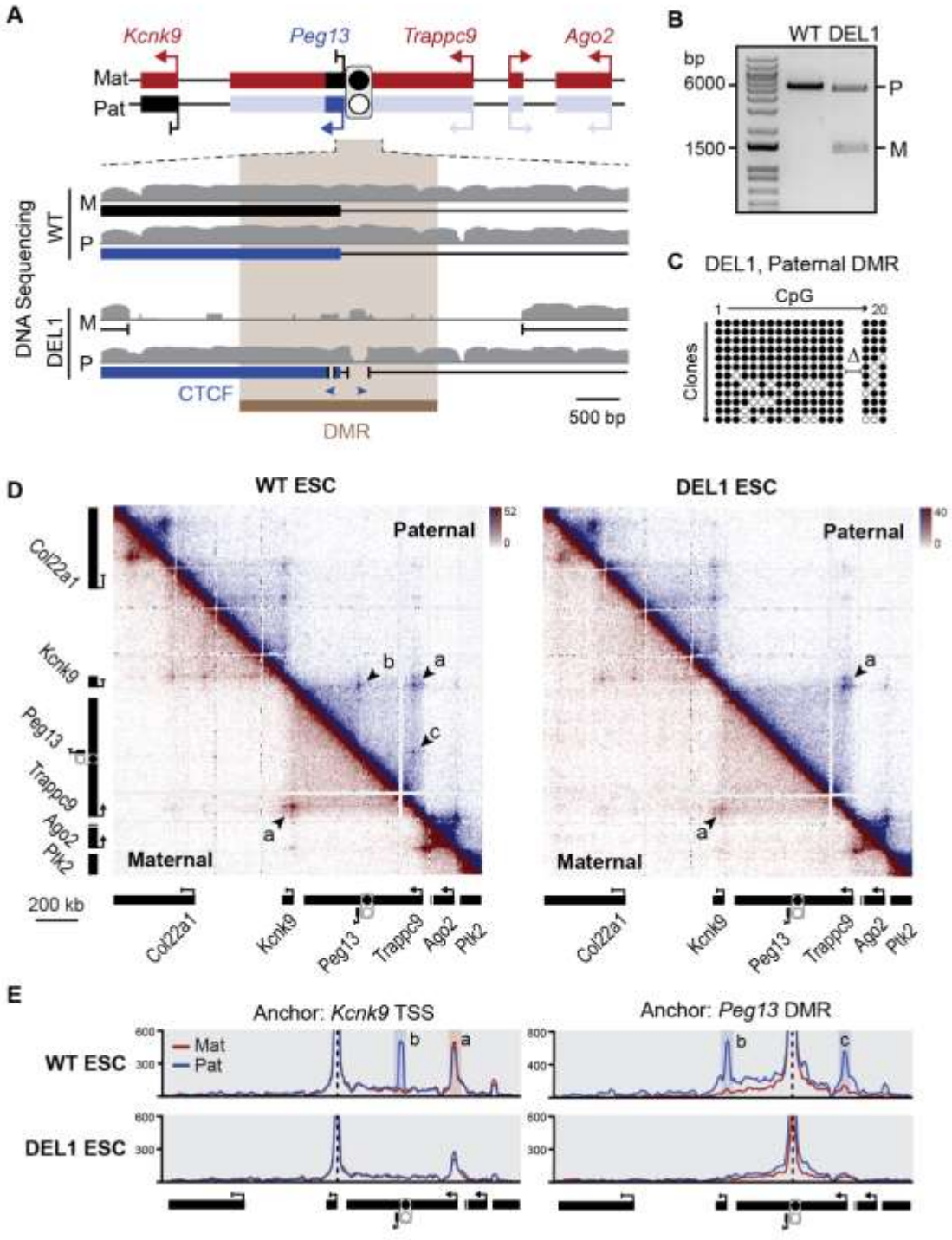

Figure 13 – Genetic and structural analysis of *Peg13* DMR DEL1

(Figure 13, continued) A. Diagram of the *Peg13* DMR depicting the CRISPR-mediated deletions of DEL1. Genomic tracks show single-end mapping of Hi-C genomic DNA. **B.** Agarose gel showing PCR products from the clonal ESC line using primers spanning the *Peg13* DMR. Deletion products were validated by Sanger sequencing to determine parent-of-origin using strain-specific SNPs. **C.** Bisulfite Sanger-sequencing across the *Peg13* DMR in DEL1 ESCs indicating methylated (closed circles) and unmethylated (open circles) CpGs. Two CpGs overlapping the deleted CTCF site are indicated with Δ. **D.** Allelic contact maps from region capture Hi-C of WT and DEL1 ESCs. Arrowheads indicate contacts of interest. **E.** Virtual 4C analysis of region capture Hi-C from WT and DEL1 ESCs.

the genomic region it is presumed to be the locus ICR, but the mechanism(s) by which the DMR may regulate the allelic expression of the surrounding protein-coding genes is not known. Within the DMR there are two CTCF motifs located approximately 300 bp apart, one in the forward orientation and one in the reverse orientation (Fig. 13A). We hypothesized that the CTCF-bound region of the DMR may be the region critical for imprinted expression.

If CTCF binding is necessary for neuron-specific imprinted expression, then deletion of the paternal DMR CTCF sites should result in a maternal-like expression pattern from the paternal allele (i.e., equal gene expression between the two alleles). We used CRISPR-Cas9 and multiplexed sgRNAs to generate two clonal paternal DMR CTCF deletion lines – DEL1 (Fig. 13) has an 18 bp deletion overlapping the reverse CTCF motif and a 180 bp deletion overlapping the forward CTCF motif (Fig. 13A,B), and DEL2 (Fig. 14) has a single 348 bp deletion, including all of the forward CTCF site and most of the reverse CTCF site (Fig. 14A,B). Both DEL lines also had large deletions on the maternal allele of ~4500 bp (DEL1) and ~1300 bp (DEL2) (Fig. 13A,B; 14A,B). Bisulfite treatment followed by Sanger sequencing of DEL ESCs revealed that the paternal allele gained methylation upon deletion of the CTCF binding sites (Fig. 13C, Fig. 14C), suggesting that CTCF maintains the unmethylated state on the paternal allele.

We asked if deleting the paternal CTCF sites at the *Peg13* DMR had an effect on the structure of the paternal allele. Region capture Hi-C on WT and DEL ESCs revealed that loss of

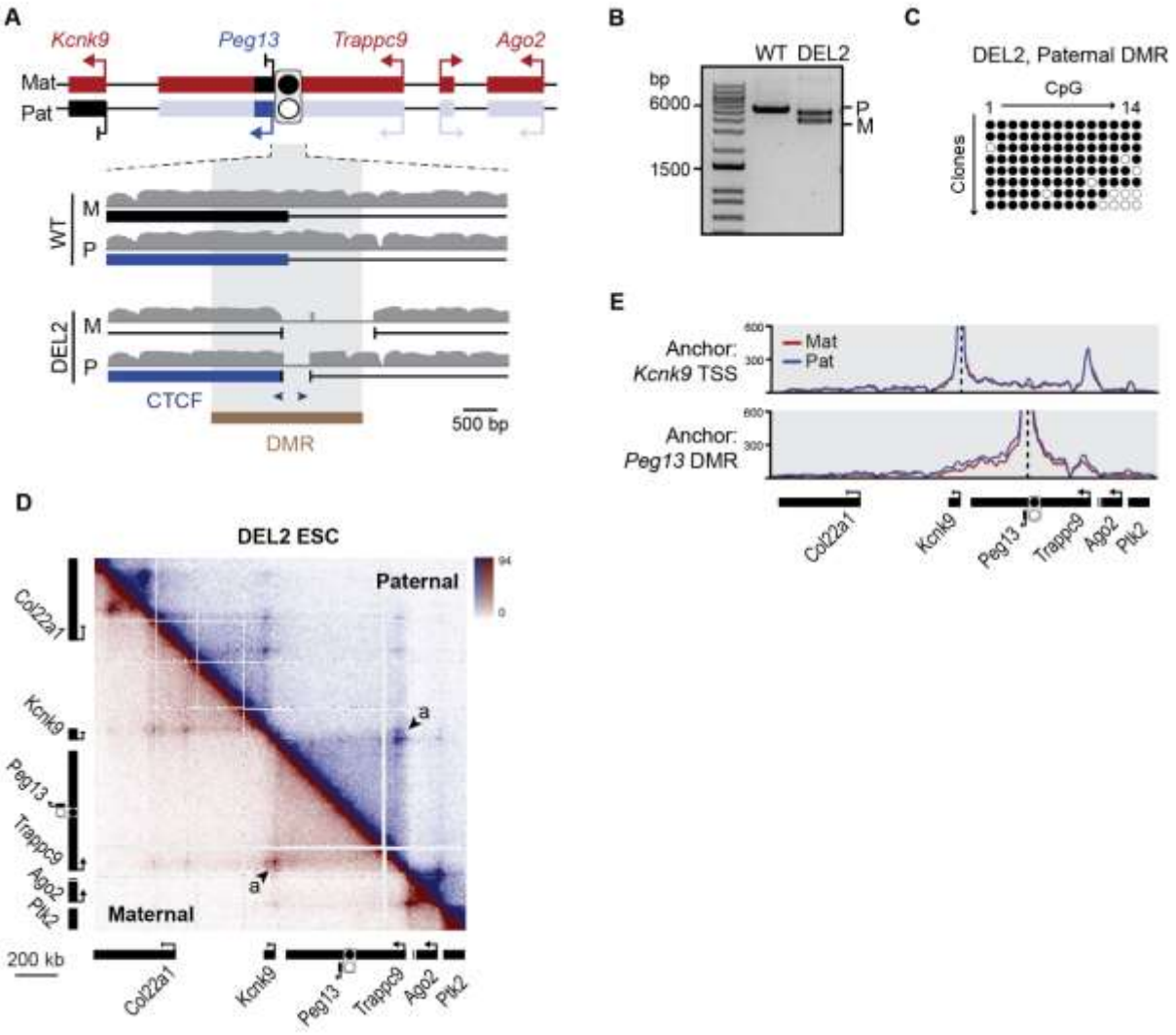

Figure 14 – Genetic and structural analysis of Peg13 DMR DEL2
A. Diagram of the *Peg13* DMR depicting the CRISPR-mediated deletions of DEL2. Genomic tracks show single-end mapping of Hi-C genomic DNA. **B.** Agarose gel showing PCR products from the clonal ESC line using primers spanning the *Peg13* DMR. Deletion products were validated by Sanger sequencing to determine parent-of-origin. **C.** Bisulfite sequencing of the DEL2 paternal DMR. **D.** Allelic region capture Hi-C of DEL2 ESCs. **E.** Virtual 4C analysis of DEL2 ESC region capture Hi-C.

paternal CTCF led to a maternalization of chromatin structure on the paternal allele, with an absence of paternal-specific sub-TADs and a strengthening of the long-range contacts crossing the *Peg13* DMR (Fig. 13D,E; Fig. 14D,E). Deletion of the methylated maternal ICR had no effect

on the chromatin structure of the maternal allele. This demonstrates that the CTCF-bound region of the *Peg13* DMR is critical for imprinted chromatin structure.

We then differentiated WT and DEL ESCs to iNs and measured total and allelic expression at the *Peg13-Kcnk9* locus (Fig. 15A,B). The DEL2 ESCs lost pluripotency and failed to properly differentiate and therefore gene expression analysis was only performed in DEL1 iNs. *Peg13* expression was strongly reduced in DEL1 iNs (Fig. 15A), reflecting the deletion of the *Peg13* TSS. *Kcnk9* expression increased approximately two-fold, consistent with an activation of paternal *Kcnk9* (Fig. 15A). The neuronal allelic biases in *Kcnk9*, *Trappc9*, and *Ago2* were significantly reduced (i.e., trended toward biallelic expression) (Fig. 15B). *Kcnk9* retained a slight maternal bias, which may reflect residual secondary epigenetic effects or additional roles for the non-deleted regions of the DMR. These results demonstrate that the *Peg13* DMR acts as the locus ICR, and that CTCF binding at the paternal DMR and/or paternal *Peg13* expression are required for imprinted expression of the locus.

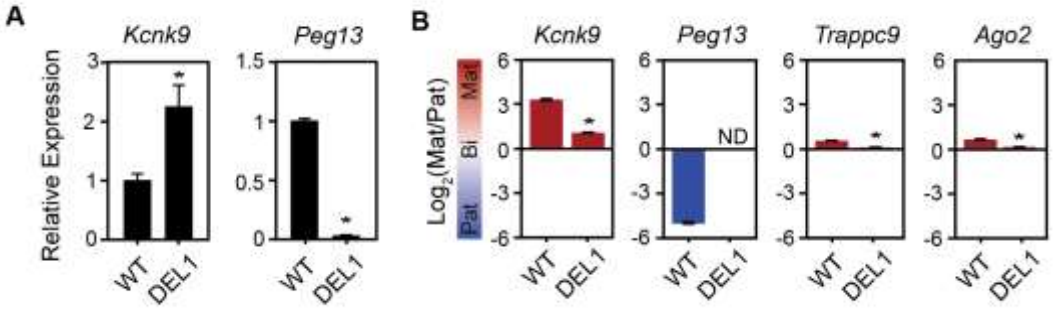

Figure 15 – Gene expression analysis of *Peg13* DMR DEL1 iNs
A. Total expression measured by RT-qPCR of WT and DEL1 iNs. Mean ± SEM (n=3). **B.** Allelic expression measured by RT-ddPCR of WT and DEL1 iNs. Mean ± SEM (n=3). *p ≤ 0.05, calculated using unpaired two-tailed Student's t-test. ND = not detected.

Peg13 lncRNA knockdown does not affect imprinted expression

Several imprinted lncRNAs, such as *Airn*, *Kcnq1ot1*, and *Ube3a-ATS,* localize to their site of transcription and act *in cis* to repress surrounding genes, either through direct transcriptional interference or by recruiting repressive factors to the locus (Pandey et al. 2008; Nagano et al. 2008; Terranova et al. 2008; Schertzer et al. 2019; Meng et al. 2013). We wanted to determine if the *Peg13* lncRNA may mediate repression of neighboring protein-coding genes on the paternal allele. The onset of *Peg13* expression on the paternal allele is correlated with the transition to maternal-biased expression of the surrounding genes during neurogenesis (Fig. 10D,E), and deletion of the *Peg13* TSS in DEL1 cells was correlated with loss of maternal-biased expression of surrounding genes. Additionally, *Peg13* has been shown to interact with the PRC2 complex (Li et al. 2023), which is responsible for deposition of the repressive H3K27me3 histone modification, further supporting this model.

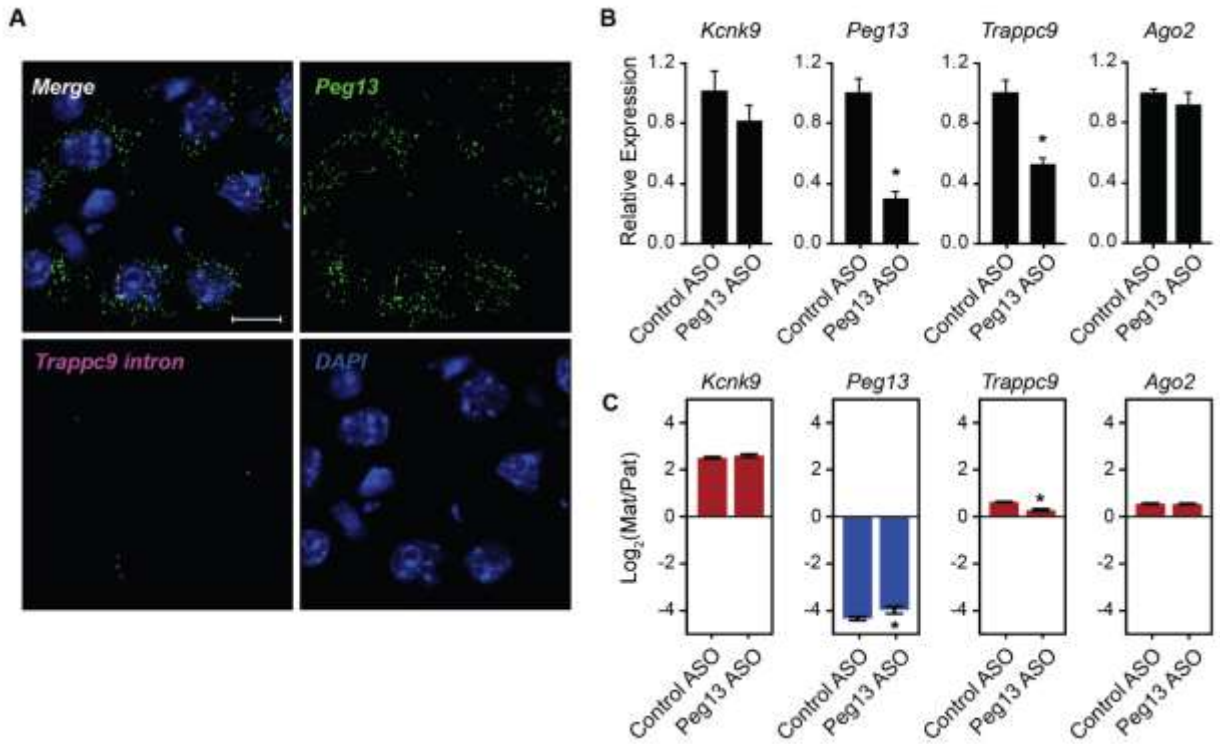

Figure 16 – *Peg13* lncRNA knockdown does not affect imprinted expression
A. Subcellular localization of *Peg13* in mouse brain sections measured using smFISH probes to *Peg13* and the neighboring intronic region of *Trappc9*. Scale bar = 10 µm. **B.** Total expression measured by RT-qPCR following ASO treatment in iNs. Mean ± SEM (n=3). **C.** Allelic

(Figure 16, continued) expression measured by RT-ddPCR following ASO treatment in iNs. Mean ± SEM (n=3). *p ≤ 0.05, calculated using unpaired two-tailed Student's t-test.

We first determined the subcellular localization of *Peg13* in mouse brain by single molecule fluorescent *in situ* hybridization (smFISH). In contrast to other cis-repressive lncRNAs (Nagano et al. 2008; Clemson et al. 1996; Mohammad et al. 2008), *Peg13* was cytoplasmic and did not form a large focus near its site of transcription (Fig. 16A). Our observation is consistent with previously published results regarding *Peg13* localization in neural stem cells (Jiang et al. 2020). Next, we tested if knockdown of *Peg13* in iNs would result in a loss of imprinted expression of the surrounding protein-coding genes. Treatment of iNs with antisense oligonucleotides (ASOs) against *Peg13* led to a ~70% knockdown of *Peg13* and a ~50% knockdown of *Trappc9* (Fig. 16B). The entire *Peg13* sequence is contained in an intron of *Trappc9* and therefore the ASOs are fully complementary to the *Trappc9* pre-mRNA; this implies the ASOs are, at least in part, knocking down nascent RNA in the nucleus. ASO treatment caused no change in either the total or allelic expression of *Kcnk9* or *Ago2* (Fig. 16B,C). These data suggest that the *Peg13* lncRNA may not be required for imprinted expression of *Kcnk9* or *Ago2* in iNs, but further experiments are required to determine if the act of transcription of *Peg13* may have cis-repressive effects on the surrounding genes.

Pre-existing allelic chromatin structure is sufficient to drive imprinted expression of *Kcnk9* upon enhancer activation

We next sought to determine the role of imprinted chromatin structure in the maternal-specific expression of *Kcnk9*. The *Kcnk9* TSS forms maternally biased contacts that cross the DMR. Potential regulatory elements located downstream of the DMR (with respect to *Kcnk9*) are insulated from *Kcnk9* on the paternal allele by the CTCF-bound DMR, making them strong

candidates for regulation of *Kcnk9* imprinted expression. This region was previously identified to have brain-specific enhancer activity in human tissue (Court et al. 2014). Analysis of publicly available ChIP-seq datasets from mouse tissues suggests that there are at least two tissue-specific, maternal enhancers in this region, which we called E1 and E2 (Fig. 17A). E1 is ~40 kb

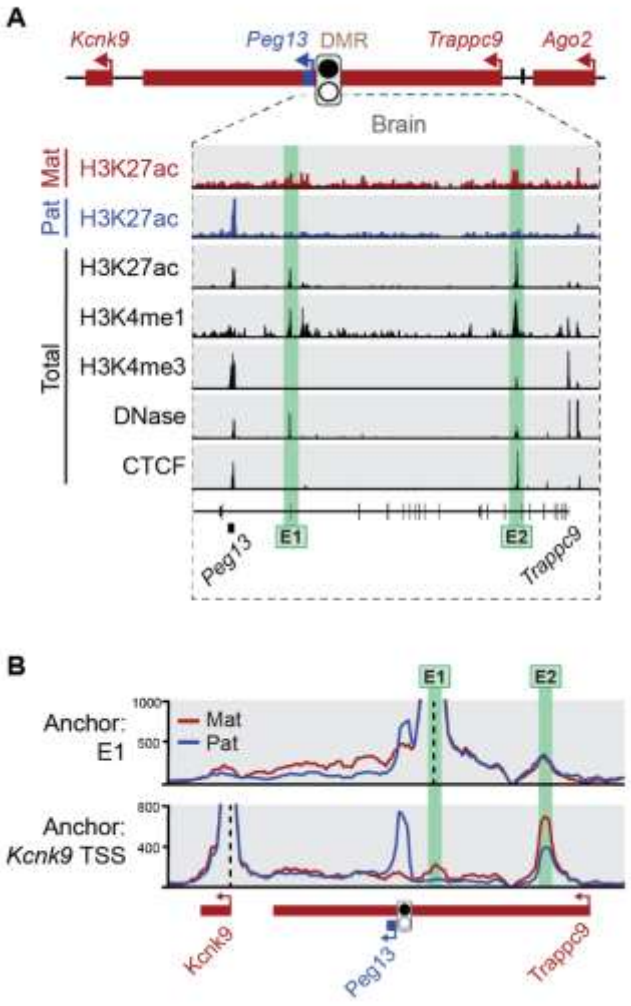

Figure 17 – Identification of putative enhancers in the *Peg13-Kcnk9* locus
A. ChIP-seq genome browser tracks from mouse brain of histone modifications, DNA accessibility, and CTCF binding at E1 and E2. Total H3K27ac, H3K4me1, H3K4me3, and CTCF ChIP-seq are from ENCODE mouse postnatal day 0 whole brain samples and allelic H3K27ac is from Xie *et al*., 2012. **B.** Virtual 4C from region capture Hi-C on hybrid mouse brain showing maternally biased contacts between the *Kcnk9* TSS and the enhancers.

downstream of the *Peg13* DMR, and E2 is adjacent to the *Trappc9* intronic CTCF site that anchors the major maternal TAD (Fig. 17A). Both enhancers have high levels of H3K27ac and H3K4me1, and low levels of H3K4me3 in mouse brain. Moreover, an allelic H3K27ac dataset from hybrid mouse brain shows a maternal bias in E1 and E2 activity. Both enhancers make maternally biased contacts with the *Kcnk9* TSS in mouse brain (Fig. 17B), further supporting their potential role in driving maternal-specific expression of *Kcnk9* in neurons. These regions do not show active enhancer marks in peripheral tissues or ESCs (Fig. 18A,B), indicating they are brain-specific enhancers with preferential activity on the maternal allele.

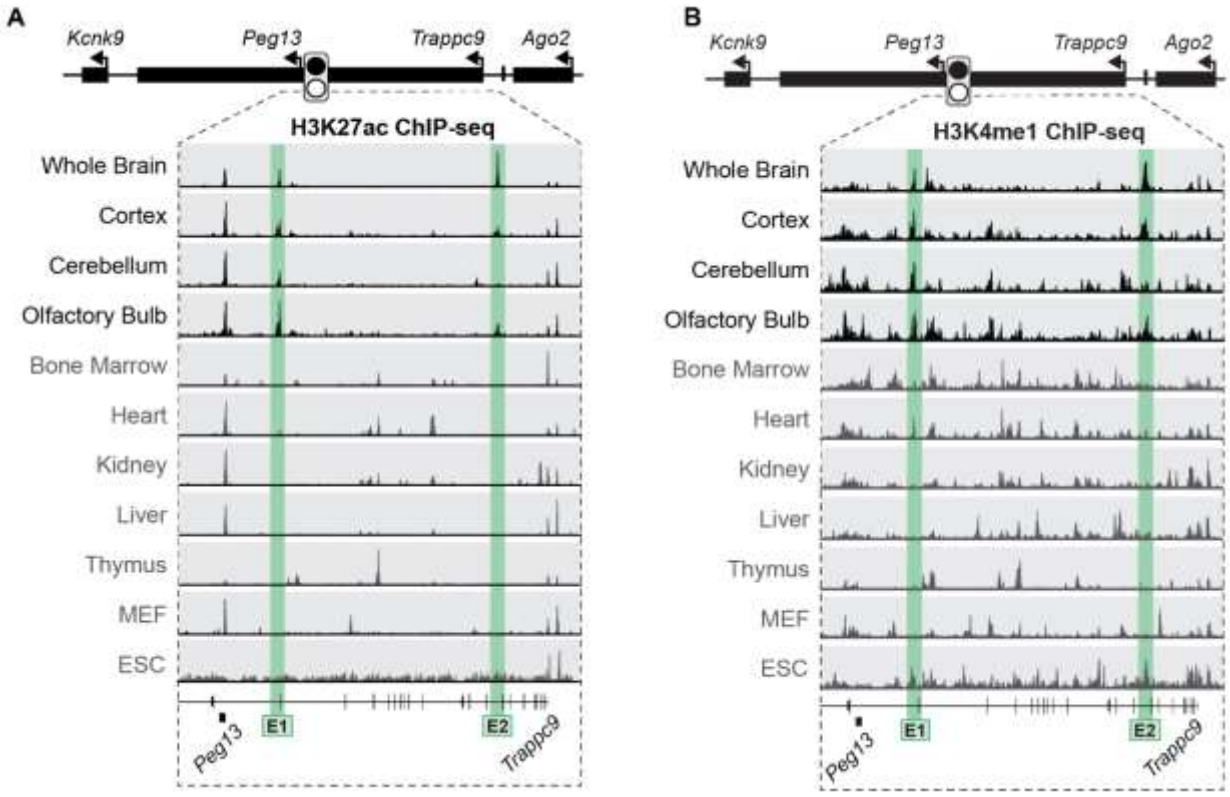

Figure 18 – Tissue specificity of putative enhancers
A. ENCODE tracks across mouse tissues for H3K27ac. **B.** ENCODE tracks across tissues for H3K4me1.

Given that allelic chromatin structure at the *Peg13-Kcnk9* locus is formed prior to the onset of *Kcnk9* expression, we hypothesized that pre-existing allelic contacts with these

enhancers may be driving maternal-specific imprinted expression of *Kcnk9* in neurons. We therefore asked if premature activation of these enhancers in the context of pre-existing allelic chromatin structure would drive maternal-specific expression of *Kcnk9*. We tested this in hybrid ESCs, which do not yet express *Kcnk9* but do have imprinted chromatin structure at the *Peg13-Kcnk9* locus. We guided biallelic transcriptional activation of the enhancers in WT ESCs using dCas9-VPR and multiplexed sgRNAs targeted to the enhancers (Fig. 19A). We then assessed the effects on gene expression in the *Peg13-Kcnk9* locus. We found that activation of E1 and E2 individually increased *Kcnk9* expression 5-fold and 25-fold, respectively. Co-activation of both enhancers simultaneously increased *Kcnk9* expression over 50-fold (Fig. 19B). This upregulation occurred in a maternally biased manner in WT ESCs (Fig. 19C). These results are not due to allelic differences in chromatin state at the *Kcnk9* promoter, as directly targeting the promoter of *Kcnk9* with dCas9-VPR led to a strong, biallelic upregulation of *Kcnk9* (Fig. 19B,C), and nanopore sequencing showed that the *Kcnk9* promoter is unmethylated on both alleles (Fig. 20A,B). This supports a model in which both alleles of *Kcnk9* are accessible and transcriptionally competent, but only the maternal allele can be induced by enhancer activation due to differential chromatin structure.

In contrast to the strong effects of enhancer activation on *Kcnk9* imprinted expression, other genes in the locus were minimally affected. E2 forms a paternal-specific contact with the *Peg13* DMR (arrowhead ‘c’ in Fig. 8C), but E2 activation by dCas9-VPR only produced a 2.5-fold upregulation of *Peg13* (Fig. 20C). A similar fold change in *Peg13* was observed using sgRNAs to the *Kcnk9* TSS. All *Peg13* expression is presumed to be on the paternal allele due to methylation of the maternal promoter. Of note, E2 activation did not increase *Trappc9* or *Ago2* expression (Fig. 20D,E) even though the promoters of these genes are hundreds of kilobases closer to the enhancer than is the *Kcnk9* promoter.

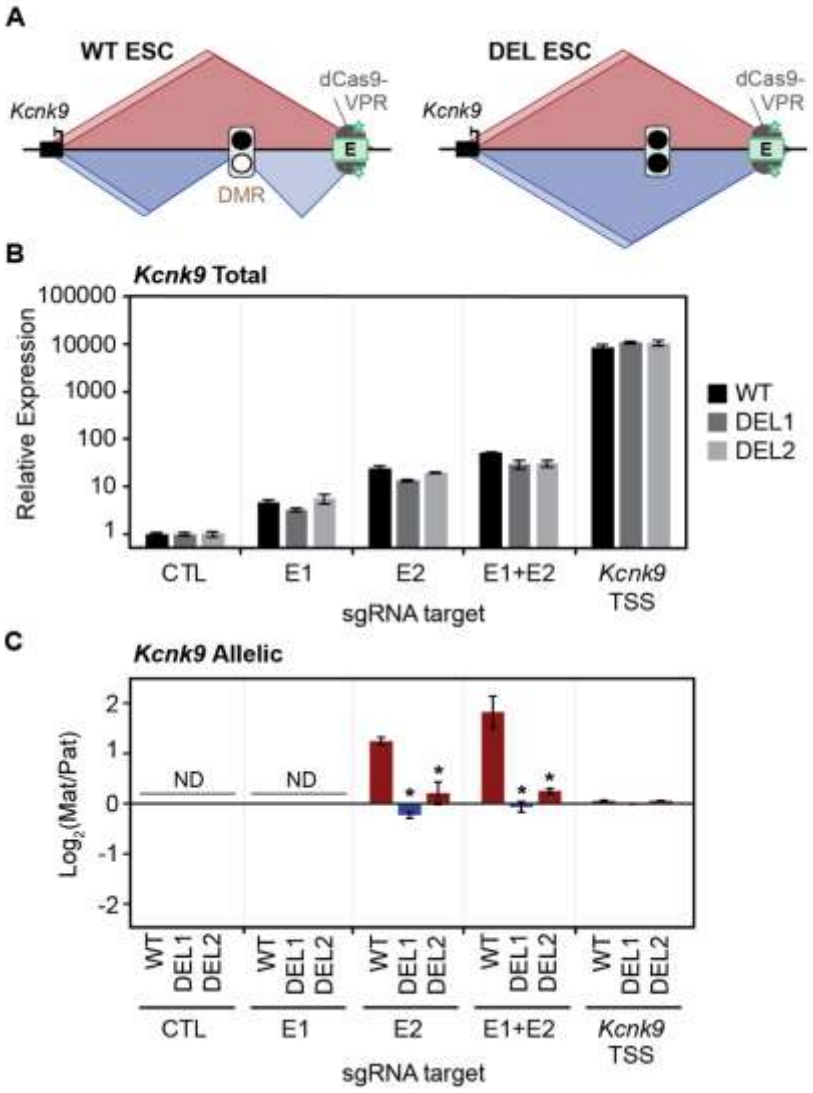

Figure 19 – Distal enhancer activation leads to imprinted expression of *Kcnk9* in an allelic chromatin structure-dependent manner

A. Diagram of CRISPR activation experimental design. dCas9-VPR was guided to the enhancers (E2 depicted) or the *Kcnk9* TSS. **B.** Total expression of *Kcnk9* as measured by RT-qPCR after guiding dCas9-VPR to the indicated target sites in WT and DEL ESCs. CTL samples were transfected with the sgRNA plasmid backbone with no sgRNAs inserted. **C.** Allelic expression of *Kcnk9* as measured by RT-ddPCR following dCas9-VPR treatment in WT and DEL ESCs. ND, not detected.

To further test this model, we then examined the effects of biallelic enhancer activation in DEL1 and DEL2 ESCs which do not have any imprinted chromatin structure or *Peg13* lncRNA. In this case, biallelic activation of the enhancers led to biallelic activation of *Kcnk9* (Fig. 19C). This demonstrates that the effect of enhancer activation on *Kcnk9* imprinted expression is dependent on allelic chromatin structure and/or *Peg13* transcription, and that pre-existing allelic chromatin structure is sufficient to drive imprinted expression of *Kcnk9* upon enhancer activation.

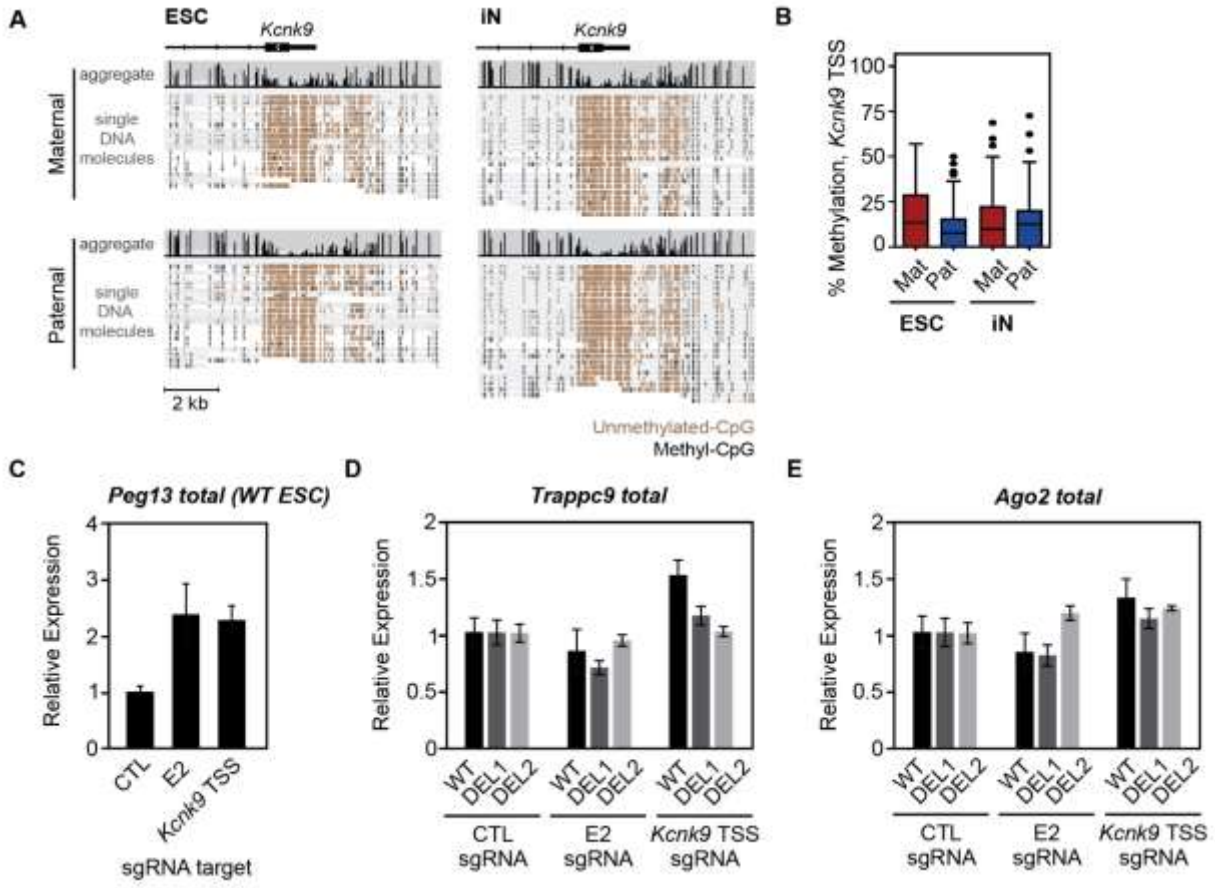

Figure 20 – Allelic promoter accessibility of *Kcnk9*
A. Targeted nanopore sequencing of native genomic DNA of the *Kcnk9* TSS to determine CpG methylation levels in WT ESCs and iNs. **B.** Quantification of (C). **C.** Total *Peg13* expression as measured by RT-qPCR after guiding dCas9-VPR to the indicated target sites in WT ESCs. Note that this was not done in DEL ESCs as the *Peg13* promoter is deleted in those cell lines. CTL samples were transfected with the sgRNA plasmid backbone with no sgRNAs inserted. **D.** Total expression of *Trappc9* as measured by RT-qPCR after guiding dCas9-VPR to the indicated

(Figure 20, continued) target sites in WT and DEL ESCs. **E.** Total expression of *Ago2* as measured by RT-qPCR after guiding dCas9-VPR to the indicated target sites in WT and DEL ESCs.

DISCUSSION

In this study, we sought to characterize the cis-regulatory mechanisms underlying brain-specific imprinted expression of the *Peg13-Kcnk9* locus. Previous work from human brain tissue showed allelic CTCF binding and enhancer blocking activity at the *Peg13* DMR and proposed a model in which higher-order chromatin structure may lead to allelic enhancer effects (Court et al. 2014). Using hybrid mouse crosses with a high density of allelic SNPs, we found that paternal-specific CTCF binding at the *Peg13* DMR leads to imprinted chromatin structure, and that this imprinted chromatin structure precedes imprinted gene expression at the locus. Then, in an *in vitro* neuron differentiation system, we showed that CTCF binding at the paternal DMR and/or paternal *Peg13* expression is required for imprinting control at the locus. Additionally, we found that enhancer activation is sufficient to drive maternal-specific expression of *Kcnk9* in a manner that is dependent on pre-existing allelic chromatin structure.

We also tested a model in which the *Peg13* lncRNA acts *in cis* to repress the surrounding genes on the paternal allele. Other imprinted lncRNAs, such as *Kcnq1ot1*, *Airn*, and *Ube3a-ATS,* mediate gene repression through mechanisms involving recruitment of cis-repressive factors (Pandey et al. 2008; Nagano et al. 2008; Terranova et al. 2008; Schertzer et al. 2019) or direct transcriptional interference (Meng et al. 2013; Latos et al. 2012; Tibbit et al. 2015). Preliminary support for this model includes i) the correlation between paternal *Peg13* induction and maternally biased expression of *Kcnk9*, *Trappc9*, and *Ago2* in the differentiation of ESCs to iNs and ii) the loss of imprinted expression in DEL1 iNs with *Peg13* TSS deletion. In contrast to other cis-repressive lncRNAs, *Peg13* is cytoplasmic. We found that ASO-mediated knockdown of the *Peg13* lncRNA did not affect the imprinted expression of *Kcnk9* or *Ago2*. It is possible that the act of transcription initiation/elongation or nascent *Peg13* RNA could play a functional role at the locus prior to export. We believe the ASOs likely reduced, to some extent, nascent *Peg13* in the nucleus given their effect on *Trappc9* pre-mRNA. This experiment

provides evidence against a cis-repressive role for *Peg13* but additional experiments are merited, such as transcriptional inhibition by premature polyadenylation site insertion or CRISPRi. Separate from any potential cis-regulatory role, other recent work has proposed that *Peg13* may act as a miRNA sponge (Jiang et al. 2020; Feng et al. 2020; Gao et al. 2022) and suppress *Yy1* through the recruitment of the PRC2 complex (Li et al. 2023).

In addition to its role in mediating allelic chromatin structure, our data also suggest that CTCF is important for maintaining an open chromatin state at the paternal *Peg13* DMR. Deleting the CTCF binding sites at the DMR led to a gain of methylation of the surrounding region, which is similar to previous observations at the *H19-Igf2* locus (Pant et al. 2004). ICR maintenance is an area of ongoing research and is not fully understood. DNA-binding proteins such as ZFP57 and TRIM28 are important for protecting ICRs from the wave of global demethylation that occurs during early embryogenesis (Li et al. 2008; Messerschmidt et al. 2012; Zuo et al. 2012; Alexander et al. 2015). CTCF is bound to the unmethylated allele of many ICRs and DMRs (Prickett et al. 2013), and it may play a part in ICR maintenance across multiple imprinted regions in addition to its role in higher-order chromatin organization.

While this work provides important insights into brain-specific imprinted expression at the *Peg13-Kcnk9* locus, several key questions remain. It remains to be determined how the imprinted biases of *Trappc9*, *Chrac1*, and *Ago2* are acquired during neuron differentiation. We did not observe a change in *Trappc9* or *Ago2* levels upon enhancer activation or *Kcnk9* TSS activation, suggesting that the mechanism underlying *Trappc9* and *Ago2* imprinted expression may be different from that of *Kcnk9*. While the imprinted expression of *Kcnk9* and *Peg13* is conserved between mouse and human (Court et al. 2014), the maternally biased expression of *Trappc9* and *Ago2* may not be (Court et al. 2014), further supporting the notion that *Trappc9* and *Ago2* imprinting may be achieved through a different mechanism than *Kcnk9*.

Genetic mutations in the *Peg13-Kcnk9* locus are associated with intellectual disability (Marangi et al. 2013; Abbasi et al. 2017; Mortreux et al. 2018; Barel et al. 2008), and our current work on the mechanistic basis of imprinting at the *Peg13-Kcnk9* locus may be informative for future therapeutic approaches. Previously, re-activation of the normally silent paternal allele of *Kcnk9* by global histone deacetylase inhibition rescued the behavioral phenotype in a Birk-Barel syndrome mouse model, a disease caused by a missense mutation in maternal *Kcnk9* (Cooper et al. 2020). In our study, we found that the paternal allele of *Kcnk9* was reactivated upon deletion of the CTCF-containing region of the DMR, highlighting additional therapeutic opportunities in Birk-Barel syndrome, for example through dCas9-mediated blocking of CTCF at the paternal DMR.

The role that higher-order chromatin structure plays in gene regulation remains a matter of debate. Many lasting features of chromatin structure are established genome-wide early in development (Collombet et al. 2020). But dynamic changes in chromatin contacts during development correlate with transcriptional changes (Bonev et al. 2017), leading to questions about the cause-effect relationship of chromatin structure and gene expression. Our data suggests a model whereby chromatin structure established early in development can prime lineage-specific gene expression patterns. Whether this mechanism will apply to other loci with tissue-specific imprinted expression remains to be seen. Our finding that allelic chromatin structure at the *Peg13-Kcnk9* locus is largely static during differentiation is consistent with recent experiments on the *Dlk1-Dio3* imprinted locus, where the paternal-specific activation of *Dlk1* upon neurogenesis occurs in the absence of corresponding changes in chromatin structure on the paternal allele (Llères et al. 2019). It will be interesting to see if this holds true for genes with more complex tissue-specific imprinted expression patterns. *Igf2* is known to be paternally expressed in early development in a chromatin-structure dependent manner, but it intriguingly switches to a maternal bias in the brain (Perez et al. 2015). Whether this happens in a static or

dynamic chromatin structure environment, or whether this switch is dependent on chromatin structure at all, remains an open question. Another example is found at the *Grb10-Ddc* locus. *Grb10* is maternally expressed in most adult tissues in mouse, but in neuronal tissue it is expressed from an alternative paternal-specific promoter (Garfield et al. 2011; Hikichi et al. 2003). The maternal-specific expression in heart and muscle is depends on allelic chromatin structure due to allelic CTCF binding at a secondary DMR (Juan et al. 2022), but the role of chromatin structure in the switch to paternal expression in neuronal lineages has not been investigated. Overall, our work contributes to an emerging model that imprinted chromatin structure may be a widespread mechanism through which epigenetic inheritance regulates gene expression across tissues.

In order to build upon this work, several additional experiments are suggested. While this work suggests a model by which higher-order chromatin structure is the main factor in mediating maternal expression of *Kcnk9*, *Trappc9*, and *Ago2*, our work leaves open the possibility of a role for other *Peg13* DMR features, most notably the *Peg13* lncRNA. Isolating the contributions of individual elements of the *Peg13* DMR is inherently challenging as it is difficult to make modifications to elements such as DNA methylation, lncRNA transcription, and CTCF binding without affecting the other components. One way to isolate the role of higher-order chromatin structure more precisely would be to build upon our work in the *Peg13* DMR neuron differentiation system. If higher-order chromatin structure is the mechanistic basis of imprinted expression at the locus, then reinsertion of a new CTCF binding site near the DMR deletion should restore allelic expression. This approach would be especially powerful as it would predict that paternal insertion of CTCF would restore proper imprinted expression, while maternal insertion would result in an inverse imprinted expression pattern, with *Kcnk9*, *Trappc9*, and *Ago2* having a paternal bias.

Additionally, further experiments are possible that would continue to test the role of the *Peg13* lncRNA in mediating imprinted expression *in cis*. The ASO KD approach that we took in this work suggests that the lncRNA is not essential for imprinted expression. However, because a cis-acting lncRNA could theoretically exert its repressive effects on local chromatin rapidly after transcription, it is conceivable that the ASO approach is not fast enough to affect this activity. As a result, a system that block *Peg13* transcription itself may be more suitable to test this model. While the straightforward deletion of the *Peg13* promoter fails in this task due to interference with other elements of the DMR, there are other possible means of achieving *Peg13* transcriptional knockdown. One possibility would be to direct CRISPRi to the promoter. While it would have to be validated that the CRISPRi system does not affect DNA methylation or CTCF binding, this would potentially be the most effective way to knock down *Peg13* expression in its entirety without a genetic deletion. Another approach would be to insert a premature polyadenylation site (PAS) downstream of the *Peg13* TSS as has been done to test other potential cis-acting lncRNAs (Engreitz et al. 2016). However, this approach would still allow for the transcription of the 5' end of *Peg13*, and so one would not be able to completely count out a role for repressive elements in this section of the lncRNA. Furthermore, because *Peg13* is internal to *Trappc9* and transcribed in a sense direction, this approach risks premature termination of paternal *Trappc9* with unpredictable effects on the broader paternal allele. While the native *Peg13* PAS apparently does not affect *Trappc9* expression, possibly due to mechanisms such as the repression of intronic PASs by the U1 snRNP (Almada et al. 2013; Ran et al. 2021), this possibility must be considered with in this approach. Overall, while our data suggest that *Peg13* is not a cis-repressive lncRNA, experiments such as those suggested here would further test this.

Overall, in this work we identify allele-specific chromatin structure at the *Peg13-Kcnk9* imprinted locus and show that this allelic chromatin structure is important for mediating

imprinted expression of the locus. More generally, we demonstrate that pre-existing chromatin structure can be important for proper regulation of developmentally regulated genes. We provide a high-resolution map of imprinted chromatin structure and a roadmap for future explorations of allele-specific chromatin structure. We provide evidence against a model in which the *Peg13* lncRNA acts *in cis* to repress surrounding chromatin, although further experiments are needed to fully eliminate this model. We also find that in addition to its function in mediating allelic chromatin structure at the *Peg13-Kcnk9* locus, allelic CTCF binding is also important for maintaining the unmethylated state on the paternal allele. Whether these findings are generalizable to other imprinted loci remains to be seen. Allelic binding of CTCF has been identified at a number of additional loci (Prickett et al. 2013), suggesting that allelic chromatin structure may a general means by which placental mammals achieve imprinted expression across broad stretches of chromatin.

METHODS

ESC line generation and culture

The ESC line used in this study were derived from an F1 *Mus. Musculus* (129/Sv) x *Mus. Castaneous* cross, F1.2-3 (Eggan et al. 2001). Two PiggyBac plasmids were co-transfected into ESCs for stable integration of EF1α-rtTA (PB-EF1α-M2rtTA;CMV-HygroR) and TetO-Ngn2 (PB-TetO-Ngn2;SV40-NeoR) in the presence of piggyBac transposase. ESCs with the integrated constructs were selected for 10 days in ESC media containing Hygromycin B (150 µg/ml) and Geneticin (300 µg/ml). A single cell ESC clonal line (F1.2-3; EF1α-rtTA;TetO-Ngn2 clone D4) with high differentiation potential and maintenance of proper imprinting at the *Peg13-Kcnk9* locus was used for all studies described here. To passage ESCs, cells were washed with HEPES-buffered saline (HBS), dissociated using 0.25% Trypsin in HBS with 1 mM EDTA, and then transferred onto plates pre-coated with 0.2% gelatin in phosphate-buffered saline (PBS). ESCs were maintained in serum/LIF ESC media composed of Dulbecco's Modified Essential Media (Thermo) supplemented with 10 mM HEPES (Thermo), 0.11 mM β-mercaptoethanol (Sigma), 1X nonessential amino acids (Corning), 2 mM L-glutamine (Corning), 1X penicillin streptomycin solution (Corning), 15% fetal bovine serum (Cytivia), and 1000 U/mL leukemia inhibitory factory (Sigma). Cells were maintained in a humidified 5% CO_2 incubator at 37°C and split every 48 hours or when cells reached 70% confluency, whichever came first.

Neuron differentiation

ESCs were cultured for 24 hours on gelatin-coated plates in ESC media (as above), then ESCs were washed and cultured for 24 hours in neuron differentiation media [BrainPhys media supplemented with 1X SM1 neuronal supplement (STEMCELL Technologies), 1X N-2 supplement (Thermo), 20 ng/mL brain-derived neurotrophic factor (STEMCELL Technologies), and 1 µg/ml doxycycline (Sigma)]. Day 1 iNs were then dissociated using accutase (STEMCELL

Technologies), counted, and plated on PEI-coated plates (0.1% PEI in borate buffer containing 50 mM boric acid and 24 mM sodium tetraborate at pH 8.4) in neuron differentiation media at a density of 40,000 cells/cm^2. Half of the media was replaced every 48 to 72 hours for a total of six days, unless otherwise noted.

RNA isolation and cDNA synthesis

Total RNA was harvested from ESCs or iNs in biological triplicate using TRIzol (Thermo) and subject to DNase treatment using TURBO DNase (Thermo). Reverse transcription was performed using SuperScript III Reverse Transcriptase (Thermo) with random hexamers.

qPCR

qPCR reactions were prepared using Power SYBR Green (Thermo) and run on the Bio-Rad CFX Opus 384 Real-Time PCR System. Relative expression was calculated using the delta-delta Ct method relative to ActB.

ddPCR

PCR primer/probe sets were designed using the Thermo Custom Taqman SNP Genotyping Assay Design Tool to overlap a *musculus*/*castaneous* SNP. Probes overlapping the *musculus* (maternal) or *castaneous* (paternal) SNP were VIC-conjugated or FAM-conjugated, respectively. Samples were prepared using ddPCR Supermix for Probes (No dUTP) (Bio-Rad). Droplets for ddPCR were generated using the Bio-Rad QX200 Droplet Generator, PCR was performed according to the Supermix protocol, and then droplets were read on the Bio-Rad QX200 Droplet Reader.

Bisulfite Sequencing

Genomic DNA was extracted from cell pellets using the Monarch gDNA Purification Kit (NEB). 2 µg of purified genomic DNA was then bisulfite converted using the EpiTect Bisulfite Kit (Qiagen).

PCR was performed on bisulfite-treated gDNA using HotStarTaq DNA polymerase (Qiagen). PCR product was then TOPO cloned (Thermo) and transformed into NEB Stable Competent *E. coli*. Individual colonies were picked and subject to Sanger sequencing of the *Peg13* DMR (see Table S2 for primer sequences). SNPs were used to identify maternal and paternal DNA fragments, and sequencing traces were analyzed using BISMA (Rohde et al. 2010) to determine the methylation status of individual CpGs.

Long-read methylome analysis

Isolated nuclei were subjected to GpC methylation using M.CviPI GpC methyltransferase (NEB), followed by proteinase K and RNaseA treatment. Genomic DNA was purified from the reaction using AMPure XP beads. A total of 6-12 µg of genomic DNA was dephosphorylated with rSAP (NEB), followed by AMPure XP beads purification. *In vitro* Cas9 incubation was performed to enrich the nanopore library for regions of interest using EnGen sgRNA synthesis kit (NEB) and Cas9 nuclease (NEB). Cleaved genomic DNA product was treated with NEBNext dA-tailing kit (NEB) and subjected to library preparation using nanopore adapter (ONT SQK-LSK109) and Quick T4 DNA ligase (NEB). Libraries were sequenced in MinION flow cell (ONT R9.4.1). Sequencing data was then mapped to a mouse genome in which *castaneous* SNPs were incorporated using minimap2 (2.24) (Li 2018). Variant tagging and haploid phasing of each sequencing read were performed using nanopolish (0.13.2) (Simpson et al. 2017) and whatshap (Patterson et al. 2015). Mapped data was split into each haplotype using bamtools (Barnett et al. 2011), and CpG methylation analysis was performed using nanopolish call-methylation package. Data was visualized in IGV (Robinson et al. 2011).

Chromatin immunoprecipitation (ChIP)

Chromatin for ChIP was prepared and sheared using the truChIP Chromatin Shearing Kit (Covaris). Cells (~5 million ESCs or iNs per biological replicate) in culture plates were fixed in

1% methanol-free formaldehyde (Thermo) at room temperature for 10 minutes and then quenched with glycine. Chromatin prepared using the truChIP kit was sheared to 500 bp in a volume of 130 µl using the Covaris S220 sonicator. Immunoprecipitation of chromatin was performed as follows. For each IP, 50 µl of protein A beads (Thermo) were prepared by washing on a magnetic stand three times using 0.1 M Na-phosphate buffer, pH 8. Beads were then suspended in 50 µl Na-Phosphate buffer and incubated at room temperature for 10 minutes with desired antibody [20 µl of CTCF antibody (Cell Signaling Technology #2899) or 11 µg of anti-rabbit IgG (Thermo)]. Antibody-conjugated beads were washed three times with Na-phosphate buffer and resuspended in 50 µl of Na-phosphate buffer. Resuspended beads were then added to 100 µl of sheared chromatin and rotated at 4°C overnight. Beads were then washed at 4°C, as follows: twice using low salt buffer (20 mM HEPES pH 8.0, 150 mM NaCl, 0.1% Triton X-100, 0.1% SDS, 2 mM EDTA), once using high salt buffer (20 mM HEPES pH 8.0, 500 mM NaCl, 0.1% Triton X-100, 0.1% SDS, 2 mM EDTA), twice using LiCl buffer (100 mM Tris-HCl pH 7.5, 0.5 M LiCl, 1% NP-40, 1% Na-deoxycholate), and twice using TE buffer (10 mM Tris pH 8.0, 1 mM EDTA). Beads were then resuspended in 250 µl elution buffer (10 mM Tris pH 8.0, 1 mM EDTA, 1% SDS) and incubated at 65°C for 30 minutes to elute. Samples were then pelleted and the supernatant was transferred to a new tube and incubated overnight at 65°C to reverse crosslinking. 250 µl of TE buffer was added to each IP, and then samples were treated with 0.2 µg/µl RNase A at 37°C for 1 hour followed by 0.2 µg/µl proteinase at 55°C for 1 hour. DNA was then purified using phenol-chloroform extraction followed by ethanol precipitation and subject to qPCR or ddPCR analysis.

Region Capture Hi-C

Hi-C libraries were generated using the Arima-HiC Kit with 3 µg of chromatin from ESCs, iNs, or mouse cortical quarters as input, each from two biological replicates (except for DEL ESCs). End repair and adapter ligation were performed using the Accel-NGS 2S DNA Library Kit (Swift

Biosciences). Agilent SureSelect probes against the *Peg13-Kcnk9* locus were designed against mm10 chr15:71850001-73350000. Probes overlapping *musculus*/*castaneous* SNPs were designed to perfectly match both genotypes (i.e. two probes per SNP) for *in vitro* experiments and B6 alone for *in vivo* experiments. End repaired and adapter ligated Hi-C libraries were then enriched using Agilent SureSelectXT HS Target Enrichment System. Enriched DNA was amplified and sequenced on Illumina NextSeq Sequencing System. Total sequencing depth was 170-190 million reads from mouse brain tissue and 20-60 million reads from cultured cells.

Region Capture Hi-C Analysis

The mm10 reference genome was N-masked at *musculus/castaneous* SNPs using SNPsplit_genome_preparation from SNPsplit (Krueger and Andrews 2016). The N-masked reference genome was then digested *in silico* according to the Arima restriction enzymes using HiCUP (Wingett et al. 2015). Bowtie2 (Langmead and Salzberg 2012) was then used to map fastq files to the digested N-masked reference genome using the HiCUP wrapper. Resulting SAM files were split into maternal and paternal reads using SNPsplit. Mapping statistics can be found in Table S1. Maternal and paternal SAM files from biological replicates and reciprocal crosses were first downsampled by random downsampling to achieve an equal number of reads from all replicates and crosses, and then the allelic SAM files from individual samples were merged by parent-of-origin. Allelic SAM files were converted to the Juicer medium format (Durand et al. 2016b) and then converted to .hic format using Juicer pre. Final Hi-C plots were visualized using Juicebox at 5 kb resolution (Durand et al. 2016a). Allelic subtraction plots were generated using Juicebox. Virtual 4C plots were generated by summing the contacts made from a 10 kb anchor point overlapping the genomic feature of interest and all surrounding genomic regions using a 5 kb sliding window at 1 kb resolution. Insulation score was determined by summing all contacts made in a sliding 200 kb window at 10 kb resolution.

Generation of sgRNA vectors

dCas9-VPR and Cas9 experiments were performed using a published multiplex four sgRNA construct system (Kabadi et al. 2014). The four sgRNAs for each of the sgRNA target sites (*Kcnk9* TSS, E1, and E2; see Table S3) were cloned into four sgRNA backbones each containing different small RNA promoters (Addgene #53186, #53187, #53188, #53189). Golden Gate cloning into pLV-GG-hUbC-dsRED (Addgene #84034) generated the final vector co-expressing four sgRNAs.

CRISPR deletion of DMR CTCF region

ESCs were co-transfected with 1000 ng of pX458 SpCas9(BB)-2A-GFP vector (Addgene #48138, contains eGFP) (Ran et al. 2013) and 500 ng of vector co-expressing four sgRNAs to the *Peg13* DMR CTCF region (contains DsRed) mixed with 3.75 µl of Lipofectamine 2000 (Thermo) in 500 µl of Opti-MEM (Thermo). The mixture was then plated into a suspension of 500,000 ESCs in 1.5 ml ESC media into individual wells of a gelatin-coated six-well culture plate. After 24 hours, fresh ESC media was added. The next day, eGFP+/DsRed+ cells were bulk sorted by FACS and expanded. Subsequently, single cells were sorted to establish clonal lines and expanded. Genomic DNA was extracted using QuickExtract (Epicentre) and PCR amplified across sgRNA sites (Table S2). PCR bands corresponding to deletion products were gel isolated and subject to Sanger sequencing. SNPs in the amplicon allowed for allelic determination of the deletion products. Wild-type clonal ESC lines were generated from the same procedure performed in the absence of sgRNA (i.e. no sgRNA vector).

CRISPR activation of dCas9-VPR

2 µg total of multiplex sgRNA vector and EF1α-dCas9-VPR-Puro vector (Addgene #99373) at a 2:1 molar ratio was mixed with 5 µl of Lipofectamine 2000 (Thermo) in 500 ul of Opti-MEM (Thermo). The mixture was then plated into a suspension of 600,000 ESCs in 1.5 ml ESC media into individual wells of a gelatin-coated six-well culture plate. Media was then changed after 24

hours to fresh ESC media. The next day, media was changed to ESC media containing 1 µg/ml puromycin. After 24 hours of drug selection, ESCs were washed and RNA was purified using TRIzol as above and subject to qPCR or ddPCR analysis. As a negative control, ESCs were generated from the same procedure performed in the absence of sgRNA (i.e. blank sgRNA backbone vector).

Analysis of allelic ChIP-seq data

To analyze previously published allelic ChIP-seq datasets from hybrid mouse brain, raw fastq files were downloaded from GSE35140 (CTCF) or GSE33722 (H3K27ac). Reads were trimmed using TrimGalore (Martin 2011) and then aligned using STAR (Dobin et al. 2013) to an mm10 genome in which *musculus/castaneous* SNPs had been N-masked using SNPsplit. Reads were then split into maternal and paternal reads using SNPsplit as above. Resulting BAM files were then converted to bigwigs using deepTools bamCoverage (Ramírez et al. 2014) and visualized in IGV.

Single molecule FISH

RNAScope was performed on 16 µm frozen adult mouse brain sections. Sections were fixed in cold 4% paraformaldehyde for 15 minutes. Sections were then progressively dehydrated in 50% ethanol, 70% ethanol, and 100% ethanol for 5 minutes each. Single molecule FISH was then performed using the RNAScope Fluorescent Multiplex Kit (ACD Bio). Sections were counterstained with DAPI and cover slipped with Aqua-Poly/Mount (Polysciences). Tissue sections were imaged on an Axioscan 7 (Zeiss) microscope with a 64X objective.

Antisense oligonucleotide knockdown

ESCs were cultured for 24 hours on gelatin-coated plates in ESC media (as above), then ESCs were washed and cultured for 24 hours in neuron differentiation media (as above). Day 1 iNs were then dissociated using accutase, counted, and plated on PEI-coated plates in neuron

differentiation media at a density of 40,000 cells/cm^2. On day 3, four ASOs against *Peg13* were added at a concentration of 2.5 μM each. iNs were harvested on day 6 and then RNA extraction, cDNA synthesis, qPCR and ddPCR were performed as above. See Table S4 for ASO sequences.

APPENDIX

Supplemental tables

Supplemental Table 1 – PCR primer sequences

Primer	Sequence
DMR bisulfite sequencing forward (WT and DEL1)	GGTTTAAAATTTTAATAAGATGGGTTAA
DMR bisulfite sequencing reverse (WT and DEL1)	ATACCCTAAAAATTACTACCTCAATAAA
DMR bisulfite sequencing forward (DEL2)	TATTTGGGTTTTTTTTGTGTTTTTT
DMR bisulfite sequencing reverse (DEL2)	CCCATCTTATTAAAATTTTAAACCTTATAT
Kcnk9 qPCR primer forward (total)	TTCCTTCTACTTCGCCATCAC
Kcnk9 qPCR primer reverse (total)	CCAGCACAGCGTAGAACATA
Peg13 qPCR primer forward (total)	CTAAGAACGTGGGTGGGATTT
Peg13 qPCR primer reverse (total)	GTGAGGCATTCTGTGGGAATA
Trappc9 qPCR primer forward (total)	GAATGACTTCCTGTGGTTAGGG
Trappc9 qPCR primer reverse (total)	CAGTTCCTCCGGGATAATGATAAA
Ago2 qPCR primer forward (total)	TTGGACATCAAACCTGAGAAATG
Ago2 qPCR primer reverse (total)	CTTCCATCAAACACTGGCTTC
Actb qPCR primer forward (total)	GACGAGGCCCAGAGCAAGAGAGG
Actb qPCR primer reverse (total)	GGTGTTGAAGGTCTCAAACATG
Kcnk9 ddPCR primer forward (allelic)	TGATCGCCTGTACCTTCACCTA
Kcnk9 ddPCR probe (allelic)	CGAGGGCGTCGAACA (VIC) CGAGGGCATCGAACA (FAM)
Kcnk9 ddPCR primer reverse (allelic)	CCTCGCGCATCTCATGGT

Supplemental Table 1 (Continued)

Peg13 ddPCR primer forward (allelic)	GGGTTTCTGCTATACCAACATCTCA
Peg13 ddPCR probe (allelic)	AGCACCAAGTGCCC (VIC) CACCAAATGCCC (FAM)
Peg13 ddPCR primer reverse (allelic)	GCGGATGCCTGCATTGTG
Trappc9 ddPCR primer forward (allelic)	GGTCTGTGGCCAGTCTTTGG
Trappc9 ddPCR probe (allelic)	CATCACCGATTGCTTC (VIC) ATCACCGACTGCTTC (FAM)
Trappc9 ddPCR primer reverse (allelic)	CAAGGTGGTAGGCCTCATCA
Ago2 ddPCR primer forward (allelic)	TGCAGCAGCACCGACA
Ago2 ddPCR probe (allelic)	TCCTGGATGATCTCC (VIC) CCTGGATAATCTCC (FAM)
Ago2 ddPCR primer reverse (allelic)	CTCGTACCATGGCAGCCA
Non-CTCF bound control qPCR primer forward	GGCAGATACAACATTCGAAACC
Non-CTCF bound control qPCR primer reverse	CAGCAGTTTGTGAGCATTCC
CTCF bound DMR qPCR primer forward	CGGCAATGCGGCAATCT
CTCF bound DMR qPCR primer reverse	CTCGTGGACTGGCGTTC
DMR ddPCR primer forward (allelic)	GGTGCGCAGCCACAC
DMR ddPCR probe (allelic)	TGGATGGAGACTTGCAGC (VIC) TGGATGGAGACCTGCAGC (FAM)
DMR ddPCR primer reverse (allelic)	CAACTCAGTGGAGCACCCTTAG
DMR deletion spanning PCR forward	CATGCTGCTCCCTTGTAAGATA
DMR deletion spanning PCR reverse	CACTGGGACTCATGTAGGATTG

Supplemental Table 1 (Continued)

Tubb3 qPCR primer forward	CCATTCTGGTGGACTTGGAA
Tubb3 qPCR primer reverse	GCACCACTCTGACCAAAGATA
Gata4 qPCR primer forward	GGGACAGCTTCAGAGCAGAC
Gata4 qPCR primer reverse	TCTCACTATGGGCACAGCAG
Nanog qPCR primer forward	CGGTGGCAGAAAAACCAGTG
Nanog qPCR primer reverse	AAGGCTTCCAGATGCGTTCA
Oct3/4 qPCR primer forward	CTCCCGAGGAGTCCCAGGACAT
Oct3/4 qPCR primer reverse	GATGGTGGTCTGGCTGAACACCT

Supplemental Table 2 – sgRNA sequences

sgRNA target	**sgRNA promoter**	**sgRNA sequence**
Peg13 DMR CTCF sites (Cas9 deletion)	hU6	GATTCTGTGGTGCCATCTAGC
	mU6	TGCGGCGCCCTCTACCGGGT
	7SK	CACAAATACTCGGTACACCG
	hH1	ACCGTGCGCCAGTCACCATTG
Kcnk9 TSS (dCas9-VPR)	hU6	ACCCGCGAATACATACACTC
	mU6	GCGCCTCAGGCAGACCAGAG
	7SK	GGGCAGGCTACTCCGAGGAC
	hH1	CGGGAGGTGGCGCGACCCAG
Peg13 DMR (dCas9-VPR)	hU6	CTCCCCGTGCCCCTAAACCA
	mU6	AATGTCCCACTATGTCTGCA

Supplemental Table 2 (Continued)

	7SK	CACAAATACTCGGTACACCG
	hH1	ACCGTGCGCCAGTCACCATTG
E1 (dCas9-VPR)	hU6	AAACGGGTTAATGGTAACCA
	mU6	TCTACCCGCTGGCTTAAGGG
	7SK	AGTTAGTTATCAGTCGGTGA
	hH1	TGCCAGTCAATGAGCTACCC
E2 (dCas9-VPR)	hU6	GCGGCACTAAGTAAAGGAGAG
	mU6	CAGGGCCAGTCAGTCCGTGG
	7SK	CCCATCAAAAAAGAAATCCG
	hH1	AGTGCATGAACACGTGTCCCA

Supplemental Table 3 – ASO sequences

ASO	**Sequence**
Peg13_ASO1	/52MOErA/*/i2MOErG/*/i2MOErG/*/i2MOErT/*/i2MOErT/*G*C*T*T*C*G*T*T*G*G*/i2MOErG/*/i2MOErT/*/i2MOErA/*/i2MOErT/*/32MOErC/
Peg13_ASO2	/52MOErC/*/i2MOErT/*/i2MOErA/*/i2MOErC/*/i2MOErA/*A*C*C*A*C*A*A*T*G*C*/i2MOErG/*/i2MOErC/*/i2MOErC/*/i2MOErT/*/32MOErA/
Peg13_ASO3	/52MOErG/*/i2MOErT/*/i2MOErG/*/i2MOErT/*/i2MOErC/*G*C*A*G*G*T*C*T*T*C*/i2MOErT/*/i2MOErA/*/i2MOErT/*/i2MOErC/*/32MOErC/
Peg13_ASO4	/52MOErC/*/i2MOErC/*/i2MOErC/*/i2MOErA/*/i2MOErA/*G*G*T*A*A*G*A*A*C*A*/i2MOErT/*/i2MOErC/*/i2MOErC/*/i2MOErG/*/32MOErT/

REFERENCES

Abbasi AA, Blaesius K, Hu H, Latif Z, Picker-Minh S, Khan MN, Farooq S, Khan MA, Kaindl AM. 2017. Identification of a novel homozygous TRAPPC9 gene mutation causing non-syndromic intellectual disability, speech disorder, and secondary microcephaly. *Am J Med Genet Part B Neuropsychiatr Genet Off Publ Int Soc Psychiatr Genet* **174**: 839–845.

Alexander KA, Wang X, Shibata M, Clark AG, García-García MJ. 2015. TRIM28 Controls Genomic Imprinting through Distinct Mechanisms during and after Early Genome-wide Reprogramming. *Cell Rep* **13**: 1194–1205.

Almada AE, Wu X, Kriz AJ, Burge CB, Sharp PA. 2013. Promoter directionality is controlled by U1 snRNP and polyadenylation signals. *Nature* **499**: 360–363.

Anaka M, Lynn A, McGinn P, Lloyd VK. 2009. Genomic Imprinting in Drosophila has properties of both mammalian and insect imprinting. *Dev Genes Evol* **219**: 59–66.

Bando Y, Hirano T, Tagawa Y. 2014. Dysfunction of KCNK potassium channels impairs neuronal migration in the developing mouse cerebral cortex. *Cereb Cortex N Y N 1991* **24**: 1017–1029.

Barel O, Shalev SA, Ofir R, Cohen A, Zlotogora J, Shorer Z, Mazor G, Finer G, Khateeb S, Zilberberg N, et al. 2008. Maternally inherited Birk Barel mental retardation dysmorphism syndrome caused by a mutation in the genomically imprinted potassium channel KCNK9. *Am J Hum Genet* **83**: 193–199.

Barlow DP, Stöger R, Herrmann BG, Saito K, Schweifer N. 1991. The mouse insulin-like growth factor type-2 receptor is imprinted and closely linked to the Tme locus. *Nature* **349**: 84–87.

Barnett DW, Garrison EK, Quinlan AR, Strömberg MP, Marth GT. 2011. BamTools: a C++ API and toolkit for analyzing and managing BAM files. *Bioinformatics* **27**: 1691–1692.

Bartolomei MS, Zemel S, Tilghman SM. 1991. Parental imprinting of the mouse H19 gene. *Nature* **351**: 153–155.

Beck D, Ben Maamar M, Skinner MK. Genome-wide CpG density and DNA methylation analysis method (MeDIP, RRBS, and WGBS) comparisons. *Epigenetics* **17**: 518–530.

Bell AC, West AG, Felsenfeld G. 1999. The Protein CTCF Is Required for the Enhancer Blocking Activity of Vertebrate Insulators. *Cell* **98**: 387–396.

Bieth E, Eddiry S, Gaston V, Lorenzini F, Buffet A, Conte Auriol F, Molinas C, Cailley D, Rooryck C, Arveiler B, et al. 2015. Highly restricted deletion of the SNORD116 region is implicated in Prader–Willi Syndrome. *Eur J Hum Genet* **23**: 252–255.

Bonev B, Mendelson Cohen N, Szabo Q, Fritsch L, Papadopoulos GL, Lubling Y, Xu X, Lv X, Hugnot J-P, Tanay A, et al. 2017. Multiscale 3D Genome Rewiring during Mouse Neural Development. *Cell* **171**: 557-572.e24.

Cassidy SB, Dykens E, Williams CA. 2000. Prader-Willi and Angelman syndromes: Sister imprinted disorders. *Am J Med Genet* **97**: 136–146.

Cattanach BM, Kirk M. 1985. Differential activity of maternally and paternally derived chromosome regions in mice. *Nature* **315**: 496–498.

Chen Z, Hagen DE, Wang J, Elsik CG, Ji T, Siqueira LG, Hansen PJ, Rivera RM. 2016. Global assessment of imprinted gene expression in the bovine conceptus by next generation sequencing. *Epigenetics* **11**: 501–516.

Chrysanthou S, Tang Q, Lee J, Taylor SJ, Zhao Y, Steidl U, Zheng D, Dawlaty MM. 2022. The DNA dioxygenase Tet1 regulates H3K27 modification and embryonic stem cell biology independent of its catalytic activity. *Nucleic Acids Res* **50**: 3169–3189.

Claringbould A, Zaugg JB. 2021. Enhancers in disease: molecular basis and emerging treatment strategies. *Trends Mol Med* **27**: 1060–1073.

Clemson CM, McNeil JA, Willard HF, Lawrence JB. 1996. XIST RNA paints the inactive X chromosome at interphase: evidence for a novel RNA involved in nuclear/chromosome structure. *J Cell Biol* **132**: 259–275.

Collombet S, Ranisavljevic N, Nagano T, Varnai C, Shisode T, Leung W, Piolot T, Galupa R, Borensztein M, Servant N, et al. 2020. Parental-to-embryo switch of chromosome organization in early embryogenesis. *Nature* **580**: 142–146.

Cooper A, Butto T, Hammer N, Jagannath S, Fend-Guella DL, Akhtar J, Radyushkin K, Lesage F, Winter J, Strand S, et al. 2020. Inhibition of histone deacetylation rescues phenotype in a mouse model of Birk-Barel intellectual disability syndrome. *Nat Commun* **11**: 480.

Court F, Camprubi C, Garcia CV, Guillaumet-Adkins A, Sparago A, Seruggia D, Sandoval J, Esteller M, Martin-Trujillo A, Riccio A, et al. 2014. The PEG13-DMR and brain-specific enhancers dictate imprinted expression within the 8q24 intellectual disability risk locus. *Epigenetics Chromatin* **7**: 5.

Cousin MA, Veale EL, Dsouza NR, Tripathi S, Holden RG, Arelin M, Beek G, Bekheirnia MR, Beygo J, Bhambhani V, et al. 2022. Gain and loss of TASK3 channel function and its regulation by novel variation cause KCNK9 imprinting syndrome. *Genome Med* **14**: 62.

Damaschke NA, Gawdzik J, Avilla M, Yang B, Svaren J, Roopra A, Luo J-H, Yu YP, Keles S, Jarrard DF. 2020. CTCF loss mediates unique DNA hypermethylation landscapes in human cancers. *Clin Epigenetics* **12**: 80.

Davidson IF, Bauer B, Goetz D, Tang W, Wutz G, Peters J-M. 2019. DNA loop extrusion by human cohesin. *Science* **366**: 1338–1345.

DeChiara TM, Robertson EJ, Efstratiadis A. 1991. Parental imprinting of the mouse insulin-like growth factor II gene. *Cell* **64**: 849–859.

Di Michele F, Chillón I, Feil R. 2023. Imprinted Long Non-Coding RNAs in Mammalian Development and Disease. *Int J Mol Sci* **24**: 13647.

Dily FL, Baù D, Pohl A, Vicent GP, Serra F, Soronellas D, Castellano G, Wright RHG, Ballare C, Filion G, et al. 2014. Distinct structural transitions of chromatin topological domains correlate with coordinated hormone-induced gene regulation. *Genes Dev* **28**: 2151–2162.

Dindot SV, Christian S, Murphy WJ, Berent A, Panagoulias J, Schlafer A, Ballard J, Radeva K, Robinson R, Myers L, et al. 2023. An ASO therapy for Angelman syndrome that targets an evolutionarily conserved region at the start of the UBE3A-AS transcript. *Sci Transl Med* **15**: eabf4077.

Dobin A, Davis CA, Schlesinger F, Drenkow J, Zaleski C, Jha S, Batut P, Chaisson M, Gingeras TR. 2013. STAR: ultrafast universal RNA-seq aligner. *Bioinformatics* **29**: 15–21.

Donnard E, Vangala P, Afik S, McCauley S, Nowosielska A, Kucukural A, Tabak B, Zhu X, Diehl W, McDonel P, et al. 2018. Comparative Analysis of Immune Cells Reveals a Conserved Regulatory Lexicon. *Cell Syst* **6**: 381-394.e7.

Durand NC, Robinson JT, Shamim MS, Machol I, Mesirov JP, Lander ES, Aiden EL. 2016a. Juicebox Provides a Visualization System for Hi-C Contact Maps with Unlimited Zoom. *Cell Syst* **3**: 99–101.

Durand NC, Shamim MS, Machol I, Rao SSP, Huntley MH, Lander ES, Aiden EL. 2016b. Juicer Provides a One-Click System for Analyzing Loop-Resolution Hi-C Experiments. *Cell Syst* **3**: 95–98.

Eggan K, Akutsu H, Loring J, Jackson-Grusby L, Klemm M, Rideout WM, Yanagimachi R, Jaenisch R. 2001. Hybrid vigor, fetal overgrowth, and viability of mice derived by nuclear cloning and tetraploid embryo complementation. *Proc Natl Acad Sci* **98**: 6209–6214.

Engel N. 2015. Imprinted X chromosome inactivation offers up a double dose of epigenetics. *Proc Natl Acad Sci U S A* **112**: 14408–14409.

Engreitz JM, Haines JE, Perez EM, Munson G, Chen J, Kane M, McDonel PE, Guttman M, Lander ES. 2016. Local regulation of gene expression by lncRNA promoters, transcription, and splicing. *Nature* **539**: 452–455.

Feng H, Gui Q, Zhu W, Wu G, Dong X, Shen M, Luo H, Xue S, Cheng Q. 2020. Long-noncoding RNA Peg13 alleviates epilepsy progression in mice via the miR-490-3p/Psmd11 axis to inactivate the Wnt/β-catenin pathway. *Am J Transl Res* **12**: 7968–7981.

Ferguson-Smith AC, Bourc'his D. 2018. The discovery and importance of genomic imprinting. *eLife* **7**: e42368.

Ferguson-Smith AC, Cattanach BM, Barton SC, Beechey CV, Surani MA. 1991. Embryological and molecular investigations of parental imprinting on mouse chromosome 7. *Nature* **351**: 667–670.

Fuks F, Hurd PJ, Deplus R, Kouzarides T. 2003a. The DNA methyltransferases associate with HP1 and the SUV39H1 histone methyltransferase. *Nucleic Acids Res* **31**: 2305–2312.

Fuks F, Hurd PJ, Wolf D, Nan X, Bird AP, Kouzarides T. 2003b. The Methyl-CpG-binding Protein MeCP2 Links DNA Methylation to Histone Methylation*. *J Biol Chem* **278**: 4035–4040.

Gao H, Zhang Y, Xue H, Zhang Q, Zhang Y, Shen Y, Bing X. 2022. Long Non-coding RNA Peg13 Alleviates Hypoxic-Ischemic Brain Damage in Neonatal Mice via miR-20a-5p/XIAP Axis. *Neurochem Res* **47**: 656–666.

Garfield AS, Cowley M, Smith FM, Moorwood K, Stewart-Cox JE, Gilroy K, Baker S, Xia J, Dalley JW, Hurst LD, et al. 2011. Distinct physiological and behavioural functions for parental alleles of imprinted Grb10. *Nature* **469**: 534–538.

Ghosh P, Dahms NM, Kornfeld S. 2003. Mannose 6-phosphate receptors: new twists in the tale. *Nat Rev Mol Cell Biol* **4**: 202–213.

Gigante S, Gouil Q, Lucattini A, Keniry A, Beck T, Tinning M, Gordon L, Woodruff C, Speed TP, Blewitt ME, et al. 2019. Using long-read sequencing to detect imprinted DNA methylation. *Nucleic Acids Res* **47**: e46.

Goday C, Esteban MR. 2001. Chromosome elimination in sciarid flies. *BioEssays* **23**: 242–250.

Gombert WM, Krumm A. 2009. Targeted Deletion of Multiple CTCF-Binding Elements in the Human C-MYC Gene Reveals a Requirement for CTCF in C-MYC Expression. *PLOS ONE* **4**: e6109.

González AJ, Setty M, Leslie CS. 2015. Early enhancer establishment and regulatory locus complexity shape transcriptional programs in hematopoietic differentiation. *Nat Genet* **47**: 1249–1259.

Gu T-P, Guo F, Yang H, Wu H-P, Xu G-F, Liu W, Xie Z-G, Shi L, He X, Jin S, et al. 2011. The role of Tet3 DNA dioxygenase in epigenetic reprogramming by oocytes. *Nature* **477**: 606–610.

Guibert S, Forné T, Weber M. 2012. Global profiling of DNA methylation erasure in mouse primordial germ cells. *Genome Res* **22**: 633–641.

Hagarman JA, Motley MP, Kristjansdottir K, Soloway PD. 2013. Coordinate Regulation of DNA Methylation and H3K27me3 in Mouse Embryonic Stem Cells. *PLOS ONE* **8**: e53880.

Haig D. 2000. The Kinship Theory of Genomic Imprinting. *Annu Rev Ecol Syst* **31**: 9–32.

Han L, Lee D-H, Szabó PE. 2008. CTCF Is the Master Organizer of Domain-Wide Allele-Specific Chromatin at the H19/Igf2 Imprinted Region. *Mol Cell Biol* **28**: 1124–1135.

Hanna CW. 2020. Placental imprinting: Emerging mechanisms and functions. *PLOS Genet* **16**: e1008709.

Héberlé É, Bardet AF. 2019. Sensitivity of transcription factors to DNA methylation. *Essays Biochem* **63**: 727–741.

Herbette M, Ross L. 2023. Paternal genome elimination: patterns and mechanisms of drive and silencing. *Curr Opin Genet Dev* **81**: 102065.

Hikichi T, Kohda T, Kaneko-Ishino T, Ishino F. 2003. Imprinting regulation of the murine Meg1 / Grb10 and human GRB10 genes; roles of brain-specific promoters and mouse-specific CTCF-binding sites. *Nucleic Acids Res* **31**: 1398–1406.

Hyle J, Zhang Y, Wright S, Xu B, Shao Y, Easton J, Tian L, Feng R, Xu P, Li C. 2019. Acute depletion of CTCF directly affects MYC regulation through loss of enhancer–promoter looping. *Nucleic Acids Res* **47**: 6699–6713.

Inoue A, Jiang L, Lu F, Suzuki T, Zhang Y. 2017. Maternal H3K27me3 controls DNA methylation-independent imprinting. *Nature* **547**: 419–424.

Isles AR. 2022. The contribution of imprinted genes to neurodevelopmental and neuropsychiatric disorders. *Transl Psychiatry* **12**: 1–8.

Jiang Y, Wang Y, Sun Y, Jiang H. 2020. Long non-coding RNA Peg13 attenuates the sevoflurane toxicity against neural stem cells by sponging microRNA-128-3p to preserve Sox13 expression. *PLOS ONE* **15**: e0243644.

Juan AM, Foong YH, Thorvaldsen JL, Lan Y, Leu NA, Rurik JG, Li L, Krapp C, Rosier CL, Epstein JA, et al. 2022. Tissue-specific Grb10/Ddc insulator drives allelic architecture for cardiac development. *Mol Cell* **82**: 3613-3631.e7.

Kabadi AM, Ousterout DG, Hilton IB, Gersbach CA. 2014. Multiplex CRISPR/Cas9-based genome engineering from a single lentiviral vector. *Nucleic Acids Res* **42**: e147.

Kota SK, Feil R. 2010. Epigenetic Transitions in Germ Cell Development and Meiosis. *Dev Cell* **19**: 675–686.

Krietenstein N, Abraham S, Venev SV, Abdennur N, Gibcus J, Hsieh T-HS, Parsi KM, Yang L, Maehr R, Mirny LA, et al. 2020. Ultrastructural Details of Mammalian Chromosome Architecture. *Mol Cell* **78**: 554-565.e7.

Krokan HE, Drabløs F, Slupphaug G. 2002. Uracil in DNA – occurrence, consequences and repair. *Oncogene* **21**: 8935–8948.

Krueger F, Andrews SR. 2016. SNPsplit: Allele-specific splitting of alignments between genomes with known SNP genotypes. *F1000Research* **5**: 1479.

Kurukuti S, Tiwari VK, Tavoosidana G, Pugacheva E, Murrell A, Zhao Z, Lobanenkov V, Reik W, Ohlsson R. 2006. CTCF binding at the H19 imprinting control region mediates maternally inherited higher-order chromatin conformation to restrict enhancer access to Igf2. *Proc Natl Acad Sci* **103**: 10684–10689.

Langmead B, Salzberg SL. 2012. Fast gapped-read alignment with Bowtie 2. *Nat Methods* **9**: 357–359.

Latos PA, Pauler FM, Koerner MV, Şenergin HB, Hudson QJ, Stocsits RR, Allhoff W, Stricker SH, Klement RM, Warczok KE, et al. 2012. Airn Transcriptional Overlap, But Not Its lncRNA Products, Induces Imprinted Igf2r Silencing. *Science* **338**: 1469–1472.

Li H. 2018. Minimap2: pairwise alignment for nucleotide sequences. *Bioinformatics* **34**: 3094–3100.

Li X, Ito M, Zhou F, Youngson N, Zuo X, Leder P, Ferguson-Smith AC. 2008. A Maternal-Zygotic Effect Gene, Zfp57, Maintains Both Maternal and Paternal Imprints. *Dev Cell* **15**: 547–557.

Li Y, Liu C, Fan H, Du Y, Zhang R, Zhan S, Zhang G, Bu N. 2023. Gli2-induced lncRNA Peg13 alleviates cerebral ischemia-reperfusion injury by suppressing Yy1 transcription in a PRC2 complex-dependent manner. *Metab Brain Dis* **38**: 1389–1404.

Li Z-K, Wang L-Y, Wang L-B, Feng G-H, Yuan X-W, Liu C, Xu K, Li Y-H, Wan H-F, Zhang Y, et al. 2018. Generation of Bimaternal and Bipaternal Mice from Hypomethylated Haploid ESCs with Imprinting Region Deletions. *Cell Stem Cell* **23**: 665-676.e4.

Lindahl T. 1993. Instability and decay of the primary structure of DNA. *Nature* **362**: 709–715.

Llères D, Moindrot B, Pathak R, Piras V, Matelot M, Pignard B, Marchand A, Poncelet M, Perrin A, Tellier V, et al. 2019. CTCF modulates allele-specific sub-TAD organization and imprinted gene activity at the mouse Dlk1-Dio3 and Igf2-H19 domains. *Genome Biol* **20**: 272.

Luo X, Zhang T, Zhai Y, Wang F, Zhang S, Wang G. 2021. Effects of DNA Methylation on TFs in Human Embryonic Stem Cells. *Front Genet* **12**: 639461.

Lupiáñez DG, Kraft K, Heinrich V, Krawitz P, Brancati F, Klopocki E, Horn D, Kayserili H, Opitz JM, Laxova R, et al. 2015. Disruptions of Topological Chromatin Domains Cause Pathogenic Rewiring of Gene-Enhancer Interactions. *Cell* **161**: 1012–1025.

Mackay DJG, Callaway JLA, Marks SM, White HE, Acerini CL, Boonen SE, Dayanikli P, Firth HV, Goodship JA, Haemers AP, et al. 2008. Hypomethylation of multiple imprinted loci in individuals with transient neonatal diabetes is associated with mutations in ZFP57. *Nat Genet* **40**: 949–951.

Mahat DB, Tippens ND, Martin-Rufino JD, Waterton SK, Fu J, Blatt SE, Sharp PA. 2023. Single-cell nascent RNA sequencing using click-chemistry unveils coordinated transcription. 2023.09.15.558015.

Marangi G, Leuzzi V, Manti F, Lattante S, Orteschi D, Pecile V, Neri G, Zollino M. 2013. TRAPPC9-related autosomal recessive intellectual disability: report of a new mutation and clinical phenotype. *Eur J Hum Genet EJHG* **21**: 229–232.

Martin M. 2011. Cutadapt removes adapter sequences from high-throughput sequencing reads. *EMBnet.journal* **17**: 10–12.

Mattei AL, Bailly N, Meissner A. 2022. DNA methylation: a historical perspective. *Trends Genet* **38**: 676–707.

Mayer W, Niveleau A, Walter J, Fundele R, Haaf T. 2000. Demethylation of the zygotic paternal genome. *Nature* **403**: 501–502.

Meng L, Person RE, Huang W, Zhu PJ, Costa-Mattioli M, Beaudet AL. 2013. Truncation of Ube3a-ATS Unsilences Paternal Ube3a and Ameliorates Behavioral Defects in the Angelman Syndrome Mouse Model. *PLOS Genet* **9**: e1004039.

Meng L, Ward AJ, Chun S, Bennett CF, Beaudet AL, Rigo F. 2015. Towards a therapy for Angelman syndrome by targeting a long non-coding RNA. *Nature* **518**: 409–412.

Messerschmidt DM, de Vries W, Ito M, Solter D, Ferguson-Smith A, Knowles BB. 2012. Trim28 Is Required for Epigenetic Stability During Mouse Oocyte to Embryo Transition. *Science* **335**: 1499–1502.

Messerschmidt DM, Knowles BB, Solter D. 2014. DNA methylation dynamics during epigenetic reprogramming in the germline and preimplantation embryos. *Genes Dev* **28**: 812–828.

Mohammad F, Pandey RR, Nagano T, Chakalova L, Mondal T, Fraser P, Kanduri C. 2008. Kcnq1ot1/Lit1 Noncoding RNA Mediates Transcriptional Silencing by Targeting to the Perinucleolar Region. *Mol Cell Biol* **28**: 3713–3728.

Monk D. 2015. Germline-derived DNA methylation and early embryo epigenetic reprogramming: The selected survival of imprints. *Int J Biochem Cell Biol* **67**: 128–138.

Moore LD, Le T, Fan G. 2013. DNA Methylation and Its Basic Function. *Neuropsychopharmacology* **38**: 23–38.

Mortreux J, Busa T, Germain DP, Nadeau G, Puechberty J, Coubes C, Gatinois V, Cacciagli P, Duffourd Y, Pinard J-M, et al. 2018. The role of CNVs in the etiology of rare autosomal recessive disorders: the example of TRAPPC9-associated intellectual disability. *Eur J Hum Genet* **26**: 143–148.

Nagano T, Mitchell JA, Sanz LA, Pauler FM, Ferguson-Smith AC, Feil R, Fraser P. 2008. The Air Noncoding RNA Epigenetically Silences Transcription by Targeting G9a to Chromatin. *Science* **322**: 1717–1720.

Nora EP, Goloborodko A, Valton A-L, Gibcus JH, Uebersohn A, Abdennur N, Dekker J, Mirny LA, Bruneau BG. 2017. Targeted Degradation of CTCF Decouples Local Insulation of Chromosome Domains from Genomic Compartmentalization. *Cell* **169**: 930-944.e22.

Otani J, Nankumo T, Arita K, Inamoto S, Ariyoshi M, Shirakawa M. 2009. Structural basis for recognition of H3K4 methylation status by the DNA methyltransferase 3A ATRX–DNMT3–DNMT3L domain. *EMBO Rep* **10**: 1235–1241.

Pandey RR, Mondal T, Mohammad F, Enroth S, Redrup L, Komorowski J, Nagano T, Mancini-DiNardo D, Kanduri C. 2008. Kcnq1ot1 Antisense Noncoding RNA Mediates Lineage-Specific Transcriptional Silencing through Chromatin-Level Regulation. *Mol Cell* **32**: 232–246.

Pant V, Kurukuti S, Pugacheva E, Shamsuddin S, Mariano P, Renkawitz R, Klenova E, Lobanenkov V, Ohlsson R. 2004. Mutation of a Single CTCF Target Site within the H19

Imprinting Control Region Leads to Loss of Igf2 Imprinting and Complex Patterns of De Novo Methylation upon Maternal Inheritance. *Mol Cell Biol* **24**: 3497–3504.

Patterson M, Marschall T, Pisanti N, van Iersel L, Stougie L, Klau GW, Schönhuth A. 2015. WhatsHap: Weighted Haplotype Assembly for Future-Generation Sequencing Reads. *J Comput Biol* **22**: 498–509.

Perez JD, Rubinstein ND, Dulac C. 2016. New Perspectives on Genomic Imprinting, an Essential and Multifaceted Mode of Epigenetic Control in the Developing and Adult Brain. *Annu Rev Neurosci* **39**: 347–384.

Perez JD, Rubinstein ND, Fernandez DE, Santoro SW, Needleman LA, Ho-Shing O, Choi JJ, Zirlinger M, Chen S-K, Liu JS, et al. 2015. Quantitative and functional interrogation of parent-of-origin allelic expression biases in the brain ed. S.B. Nelson. *eLife* **4**: e07860.

Prickett AR, Barkas N, McCole RB, Hughes S, Amante SM, Schulz R, Oakey RJ. 2013. Genome-wide and parental allele-specific analysis of CTCF and cohesin DNA binding in mouse brain reveals a tissue-specific binding pattern and an association with imprinted differentially methylated regions. *Genome Res* **23**: 1624–1635.

Raissig MT, Baroux C, Grossniklaus U. 2011. Regulation and Flexibility of Genomic Imprinting during Seed Development. *Plant Cell* **23**: 16–26.

Ramírez F, Dündar F, Diehl S, Grüning BA, Manke T. 2014. deepTools: a flexible platform for exploring deep-sequencing data. *Nucleic Acids Res* **42**: W187–W191.

Ran FA, Hsu PD, Wright J, Agarwala V, Scott DA, Zhang F. 2013. Genome engineering using the CRISPR-Cas9 system. *Nat Protoc* **8**: 2281–2308.

Ran Y, Deng Y, Yao C. 2021. U1 snRNP telescripting: molecular mechanisms and beyond. *RNA Biol* **18**: 1512–1523.

Rao SSP, Huntley MH, Durand NC, Stamenova EK, Bochkov ID, Robinson JT, Sanborn AL, Machol I, Omer AD, Lander ES, et al. 2014. A 3D Map of the Human Genome at Kilobase Resolution Reveals Principles of Chromatin Looping. *Cell* **159**: 1665–1680.

Ren W, Fan H, Grimm SA, Guo Y, Kim JJ, Yin J, Li L, Petell CJ, Tan X-F, Zhang Z-M, et al. 2020. Direct readout of heterochromatic H3K9me3 regulates DNMT1-mediated maintenance DNA methylation. *Proc Natl Acad Sci* **117**: 18439–18447.

Richer S, Tian Y, Schoenfelder S, Hurst L, Murrell A, Pisignano G. 2023. Widespread allele-specific topological domains in the human genome are not confined to imprinted gene clusters. *Genome Biol* **24**: 40.

Robinson JT, Thorvaldsdóttir H, Winckler W, Guttman M, Lander ES, Getz G, Mesirov JP. 2011. Integrative genomics viewer. *Nat Biotechnol* **29**: 24–26.

Rohde C, Zhang Y, Reinhardt R, Jeltsch A. 2010. BISMA - Fast and accurate bisulfite sequencing data analysis of individual clones from unique and repetitive sequences. *BMC Bioinformatics* **11**: 230.

Ruf N, Bähring S, Galetzka D, Pliushch G, Luft FC, Nürnberg P, Haaf T, Kelsey G, Zechner U. 2007. Sequence-based bioinformatic prediction and QUASEP identify genomic imprinting of the KCNK9 potassium channel gene in mouse and human. *Hum Mol Genet* **16**: 2591–2599.

Sanli I, Lalevée S, Cammisa M, Perrin A, Rage F, Llères D, Riccio A, Bertrand E, Feil R. 2018. Meg3 Non-coding RNA Expression Controls Imprinting by Preventing Transcriptional Upregulation in cis. *Cell Rep* **23**: 337–348.

Schertzer MD, Braceros KCA, Starmer J, Cherney RE, Lee DM, Salazar G, Justice M, Bischoff SR, Cowley DO, Ariel P, et al. 2019. lncRNA-Induced Spread of Polycomb Controlled by Genome Architecture, RNA Abundance, and CpG Island DNA. *Mol Cell* **75**: 523-537.e10.

Seisenberger S, Andrews S, Krueger F, Arand J, Walter J, Santos F, Popp C, Thienpont B, Dean W, Reik W. 2012. The Dynamics of Genome-wide DNA Methylation Reprogramming in Mouse Primordial Germ Cells. *Mol Cell* **48**: 849–862.

Simpson JT, Workman RE, Zuzarte PC, David M, Dursi LJ, Timp W. 2017. Detecting DNA cytosine methylation using nanopore sequencing. *Nat Methods* **14**: 407–410.

Singh P, Lee D-H, Szabo P. 2012. More than insulator: multiple roles of CTCF at the H19-Igf2 imprinted domain. *Front Genet* **3**: 214.

Singh P, Wu X, Lee D-H, Li AX, Rauch TA, Pfeifer GP, Mann JR, Szabó PE. 2011. Chromosome-Wide Analysis of Parental Allele-Specific Chromatin and DNA Methylation. *Mol Cell Biol* **31**: 1757–1770.

Smallwood SA, Tomizawa S, Krueger F, Ruf N, Carli N, Segonds-Pichon A, Sato S, Hata K, Andrews SR, Kelsey G. 2011. Dynamic CpG island methylation landscape in oocytes and preimplantation embryos. *Nat Genet* **43**: 811–814.

Smith RJ, Dean W, Konfortova G, Kelsey G. 2003. Identification of Novel Imprinted Genes in a Genome-Wide Screen for Maternal Methylation. *Genome Res* **13**: 558–569.

Smith ZD, Chan MM, Mikkelsen TS, Gu H, Gnirke A, Regev A, Meissner A. 2012. A unique regulatory phase of DNA methylation in the early mammalian embryo. *Nature* **484**: 339–344.

Spicuglia S, Vanhille L. 2012. Chromatin signatures of active enhancers. *Nucleus* **3**: 126–131.

Statello L, Guo C-J, Chen L-L, Huarte M. 2021. Gene regulation by long non-coding RNAs and its biological functions. *Nat Rev Mol Cell Biol* **22**: 96–118.

Suzuki S, Shaw G, Kaneko-Ishino T, Ishino F, Renfree MB. 2011. The Evolution of Mammalian Genomic Imprinting Was Accompanied by the Acquisition of Novel CpG Islands. *Genome Biol Evol* **3**: 1276–1283.

Szabó PE, Tang S-HE, Rentsendorj A, Pfeifer GP, Mann JR. 2000. Maternal-specific footprints at putative CTCF sites in the H19 imprinting control region give evidence for insulator function. *Curr Biol* **10**: 607–610.

Tan L, Xing D, Chang C-H, Li H, Xie XS. 2018. Three-dimensional genome structures of single diploid human cells. *Science* **361**: 924–928.

Terranova R, Yokobayashi S, Stadler MB, Otte AP, van Lohuizen M, Orkin SH, Peters AHFM. 2008. Polycomb Group Proteins Ezh2 and Rnf2 Direct Genomic Contraction and Imprinted Repression in Early Mouse Embryos. *Dev Cell* **15**: 668–679.

Tibbit CJ, Williamson CM, Mehta S, Ball ST, Chotalia M, Nottingham WT, Eaton SA, Quwailid MM, Teboul L, Kelsey G, et al. 2015. Antisense Activity across the Nesp Promoter is Required for Nespas-Mediated Silencing in the Imprinted Gnas Cluster. *Non-Coding RNA* **1**: 246–265.

Tucci V, Isles AR, Kelsey G, Ferguson-Smith AC, Tucci V, Bartolomei MS, Benvenisty N, Bourc'his D, Charalambous M, Dulac C, et al. 2019. Genomic Imprinting and Physiological Processes in Mammals. *Cell* **176**: 952–965.

Ushiki A, Zhang Y, Xiong C, Zhao J, Georgakopoulos-Soares I, Kane L, Jamieson K, Bamshad MJ, Nickerson DA, Shen Y, et al. 2021. Deletion of CTCF sites in the SHH locus alters enhancer–promoter interactions and leads to acheiropodia. *Nat Commun* **12**: 2282.

Vangala P, Murphy R, Quinodoz SA, Gellatly K, McDonel P, Guttman M, Garber M. 2020. High-Resolution Mapping of Multiway Enhancer-Promoter Interactions Regulating Pathogen Detection. *Mol Cell* **80**: 359-373.e8.

Wang H, Maurano MT, Qu H, Varley KE, Gertz J, Pauli F, Lee K, Canfield T, Weaver M, Sandstrom R, et al. 2012. Widespread plasticity in CTCF occupancy linked to DNA methylation. *Genome Res* **22**: 1680–1688.

Wang J, Hevi S, Kurash JK, Lei H, Gay F, Bajko J, Su H, Sun W, Chang H, Xu G, et al. 2009. The lysine demethylase LSD1 (KDM1) is required for maintenance of global DNA methylation. *Nat Genet* **41**: 125–129.

Wang S, Su J-H, Beliveau BJ, Bintu B, Moffitt JR, Wu C, Zhuang X. 2016. Spatial organization of chromatin domains and compartments in single chromosomes. *Science* **353**: 598–602.

Whipple AJ, Breton-Provencher V, Jacobs HN, Chitta UK, Sur M, Sharp PA. 2020. Imprinted Maternally Expressed microRNAs Antagonize Paternally Driven Gene Programs in Neurons. *Mol Cell* **78**: 85-95.e8.

Williamson CM, Turner MD, Ball ST, Nottingham WT, Glenister P, Fray M, Tymowska-Lalanne Z, Plagge A, Powles-Glover N, Kelsey G, et al. 2006. Identification of an imprinting control region affecting the expression of all transcripts in the Gnas cluster. *Nat Genet* **38**: 350–355.

Wingett S, Ewels P, Furlan-Magaril M, Nagano T, Schoenfelder S, Fraser P, Andrews S. 2015. HiCUP: pipeline for mapping and processing Hi-C data. *F1000Research* **4**: 1310.

Xie W, Barr CL, Kim A, Yue F, Lee AY, Eubanks J, Dempster EL, Ren B. 2012. Base-Resolution Analyses of Sequence and Parent-of-Origin Dependent DNA Methylation in the Mouse Genome. *Cell* **148**: 816–831.

Zuin J, Roth G, Zhan Y, Cramard J, Redolfi J, Piskadlo E, Mach P, Kryzhanovska M, Tihanyi G, Kohler H, et al. 2022. Nonlinear control of transcription through enhancer–promoter interactions. *Nature* **604**: 571–577.

Zuo X, Sheng J, Lau H-T, McDonald CM, Andrade M, Cullen DE, Bell FT, Iacovino M, Kyba M, Xu G, et al. 2012. Zinc Finger Protein ZFP57 Requires Its Co-factor to Recruit DNA Methyltransferases and Maintains DNA Methylation Imprint in Embryonic Stem Cells via Its Transcriptional Repression Domain*. *J Biol Chem* **287**: 2107–2118.